NTNU – Trondheim
Norwegian University of
Science and Technology

Investigating the Local Load Sharing Fibre Bundle Model in Higher Dimensions

Jonas T. Kjellstadli

MSc in Physics
Submission date: May 2015
Supervisor: Alex Hansen, IFY

Norwegian University of Science and Technology
Department of Physics

Abstract

We introduce a generalization of the history-independent local load sharing fibre bundle model that is valid in arbitrarily high dimensions, and study this model numerically in one to five dimensions.

Simulations show that as the dimension D increases, the local load sharing model behaves more and more like the equal load sharing fibre bundle model. The area under the difference between their averaged strain curves, $\Delta\sigma_2$, follows a power law $\Delta\sigma_2 \propto D^{-\mu}$, indicating an infinite critical dimension where the two models converge. The exponent is estimated to be $\mu = 3.4 \pm 0.2$ for the uniform threshold distribution $P(x) = x$ and $\mu = 3.7 \pm 0.3$ for $P(x) = 1 - \exp(-x)$, both in the limit of large fibre bundles.

The burst size distribution $D(\Delta)$ when $P(x) = x$ is studied for bundle sizes of order $N \sim 10^4$ in one through five dimensions. A sudden, qualitative shift is seen when going from one to two dimensions, with the power law behaviour $D(\Delta) \propto \Delta^{-\xi}$ valid for sufficiently small bursts Δ giving an exponent $\xi \approx 4.6$ in one dimension and $\xi \approx 2.6$ in higher dimensions. Additionally, the higher dimensions retain a power law-like behaviour for much larger bursts than in one dimension, where the burst size distribution begins to deviate from a power law even for very small bursts.

Sammendrag

Vi introduserer en generalisering av den historieuavhengige lokale fiberbuntmodellen som er gyldig i vilkårlig høye dimensjoner og studerer denne modellen i én til fem dimensjoner.

Simuleringer viser at når dimensjonen D øker oppfører den lokale modellen seg mer og mer som den demokratiske fiberbuntmodellen. Arealet under kurven som uttrykker den gjennomsnittlige differansen mellom kraften som trengs for å bryte ned fiberbunten for de to modellene, $\Delta\sigma_2$, følger en potenslov $\Delta\sigma_2 \propto D^{-\mu}$. Dette indikerer en uendelig kritisk dimensjon der de to modellene kovergerer. Eksponenten estimeres til å være $\mu = 3.4 \pm 0.2$ for den uniforme fordelingen $P(x) = x$ og $\mu = 3.7 \pm 0.3$ for $P(x) = 1 - \exp(-x)$, begge i grensen når buntstørrelsen går mot uendelig.

Glippfordelingen $D(\Delta)$ blir studert for buntstørrelser av orden $N \sim 10^4$ i én til fem dimensjoner med den uniforme fordelingen $P(x) = x$. En plutselig, kvalitativ endring er synlig når man går fra én til to dimensjoner; potenslovoppførselen $D(\Delta) \propto \Delta^{-\xi}$ som er gyldig for tilstrekkelig små glipp Δ gir eksponenten $\xi \approx 4.6$ i én dimensjon og $\xi \approx 2.6$ i to og høyere dimensjoner. I høyere dimensjoner beholdes i tillegg en potenslovlignende oppførsel for mye større glipp enn i én dimensjon, der glippfordelingen begynner å avvike betydelig fra en potenslov selv for svært små glipp.

Preface

This thesis is the last part of my Master of Science in Physics degree at NTNU, the Norwegian University of Science and Technology. The work has been carried out under the supervision of Prof. Alex Hansen at the Department of Physics, and is equivalent to one academic year of work, i.e. 60 ECTS credits.

I would like to thank Alex for offering a project that has been both challenging and interesting, and for the invaluable advice and suggestions provided throughout the process of working on this thesis. Additionally, I want to thank the Department of Physics for providing computational resources, without which this thesis would not have been written.

Personally, I would like to thank my family: my father for understanding what I do, and my mother and sister for managing to find it impressive even though they don't understand it. I also want to thank my friends for providing continual support and motivation.

Trondheim, May 15, 2015

Jonas T. Kjellstadli

Contents

Abstract . . . i
Sammendrag . . . iii
Preface . . . v

1 Introduction **1**

2 Fibre bundle models **3**
2.1 Both models . . . 3
  2.1.1 Threshold distribution . . . 3
  2.1.2 Strain curve . . . 5
  2.1.3 Burst size distribution . . . 5
  2.1.4 Dimensionality . . . 5
2.2 Equal load sharing . . . 6
  2.2.1 Force distribution . . . 6
  2.2.2 Strain curve . . . 6
  2.2.3 Burst size distribution . . . 7
  2.2.4 Higher dimensions . . . 7
2.3 Local load sharing . . . 7
  2.3.1 Force distribution . . . 8
  2.3.2 Strain curve . . . 8
  2.3.3 Burst size distribution . . . 9
  2.3.4 Generalization to higher dimensions . . . 10

3 Algorithms and simulations **11**
3.1 Finding holes and perimeters . . . 11
  3.1.1 Determining hole structure . . . 11
  3.1.2 Perimeters and hole sizes . . . 13
  3.1.3 Comments . . . 13
3.2 Simulations . . . 14
  3.2.1 Parallelization . . . 14

4 Results **15**
4.1 One dimension . . . 15
  4.1.1 Strain curves . . . 15
  4.1.2 Burst size distribution . . . 16
4.2 Size dependence in four dimensions . . . 17
  4.2.1 Analytical ELS results . . . 17
  4.2.2 Numerical ELS results . . . 20
4.3 Dimensional dependence of strain curves . . . 22
  4.3.1 Uniform distribution . . . 24
  4.3.2 Exponential distribution . . . 28
4.4 Burst size distribution in higher dimensions . . . 33

5 Discussion **37**
5.1 One-dimensional results . . . 37
5.1.1 Strain curves . . . 37
5.1.2 ELS burst size distribution . . . 37
5.1.3 LLS burst size distribution . . . 38
5.1.4 Overall remarks . . . 38
5.2 Size dependence in four dimensions . . . 38
5.2.1 Analytical ELS . . . 39
5.2.2 Numerical ELS . . . 39
5.2.3 Validity . . . 39
5.3 Dimensional dependence of strain curves . . . 39
5.3.1 Uniform distribution . . . 40
5.3.2 Exponential distribution with $\mathbf{x}_< = \mathbf{0}$ . . . 41
5.3.3 Exponential distribution with $\mathbf{x}_< = \mathbf{1}$ . . . 41
5.4 Burst size distribution in higher dimensions . . . 42
5.5 Errors and inaccuracies . . . 42

6 Conclusion **45**
6.1 Suggestions for future work . . . 46

A Article **51**

1 Introduction

The strength of a material under an applied external load has been studied at length for many different materials. Theoretical descriptions and models of polymeric materials, for instance, are usually macroscopic even when the interactions between the microscopic constituent particles of the materials are fairly well known. This is because modelling a material from the bottom up to describe macroscopic failure is exceedingly difficult – even macroscopic descriptions quickly become complicated [1] – although the increase in computer power in later years has provided the means to help compute such descriptions numerically [2, 3].

Due to this lack of microscopic descriptions, the heuristic fibre bundle models have gained widespread use when studying fracture in various materials and have for instance been used to help describe for instance fibre-reinforced ceramic-matrix composites [4] and collagen fibres [5] in recent years. They are the simplest available models to study phenomena occurring in failure processes of real materials, like fatigue failure [6], similar to how the Ising model is the simplest model to study magnetic materials.

The fibre bundle models, which we will discuss in detail later, describe a system – called a bundle – of fibres subject to an external force. There are two extremes in the way forces is distributed among the fibres in the bundle, called equal and local load sharing. In local load sharing the forces from failed fibres are distributed only on their nearest neighbours, which one can think of as a nearest neighbour interaction in the bundle. Equal load sharing, on the other hand, distributes forces equally among the surviving fibres no matter where the broken fibres are placed in the bundle. In this sense it can be considered the mean field model of local load sharing, where the interactions between neighbours are replaced by an average interaction spanning the entire bundle.

When considering mean field theories the concept of an upper critical dimension, above which the critical exponents of the mean field theory are identical to the exponents of the exact theory, is important. For many models this dimension in both finite and quite small; the Ising model has an upper critical dimension of 4, for example [7].

Encouraged by this and the fact that the local load sharing model in two dimensions has been observed to give results much closer to equal load sharing than in one dimension [8], we want to investigate how the difference between the two models behave as the dimension increases. More specifically, in this thesis we want to:

- Investigate whether there is a finite critical dimension where the averaged strain curves of equal and local load sharing models converge.
- If such a dimension exists, try to find a qualitative explanation of why.

A positive result should also apply to any model somewhere in between the equal and local load sharing models; any model that distributes forces from failed fibres to more than just nearest neighbours is bound to act more like the equal load sharing model than local load sharing does, and must then also have a finite critical dimension.

As the equal load sharing model is much easier to work with analytically, and also requires much less computational power to simulate, the discovery of a finite critical dimension could aid work involving the local load sharing model. It might be possible, for example, to do an expansion from the critical dimension to lower dimensions, analogous to the results for $4 - \epsilon$ dimensions for the Ising model [9].

This thesis is organized in the following way: Chapter 1 is the introduction you are now reading. In Chapter 2 we present the fibre bundle models that are used, focusing on strain curves, burst size distributions and how both the equal and local load sharing models are described in higher dimensions. Details about the simulations and the algorithms used are found in Chapter 3. Chapter 4 presents the results obtained from the simulations, which are then discussed and interpreted in Chapter 5. Finally, Chapter 6 contains a conclusion based on the discussion and also suggests a few prospects for future work that seem interesting in the light of the presented results.

2 Fibre bundle models

The treatment of fibre bundle models (FBMs) in modern science began in 1926 when Pierce wanted to describe cotton yarns [10]. Since then a lot has happened and several variations of the models have been introduced, differing in for instance the way force is distributed among the fibres or the inclusion of thermal fluctuations. They all, however, describe the behaviour of a bundle of elastic fibres when subjected to an external force, and have proved useful in describing a wide array of physical problems, mainly regarding fracture of various materials [6].

This chapter will describe the fibre bundle models we are using. Section 2.2 and 2.3 consider the specifics of the equal load sharing and local load sharing models, respectively, while Section 2.1 describes the common elements of both models. For the specifics we mention force distribution, strain curves, the burst size distribution, and how the models are handled higher dimensions.

2.1 Both models

We consider a fibre bundle consisting of N elastic fibres attached at each end to a clamp and let $k \leq N$ denote the number of broken fibres. The set-up is shown in Fig. 2.1 for one dimension. Each fibre is assumed to act as a Hookean spring until it reaches a certain extension, x_i for fibre number i, where it breaks and is unable to carry a force any more:

$$f_i = \begin{cases} \kappa x & x < x_i \\ 0 & x \geq x_i . \end{cases} \tag{2.1}$$

Here f_i is the force the fibre exerts, x is the extension of the fibre from equilibrium, and κ is the elastic constant of the fibres. One could let the fibres have different elastic constants – either as a discrete set of values or continuously distributed according to a probability distribution – but we will not consider this.

2.1.1 Threshold distribution

The thresholds x_i are drawn from a probability density $p(x)$, often denoted by its corresponding cumulative probability distribution $P(x)$. It is called the threshold distribution to signify that it is the distribution from which the fibre thresholds are drawn.

$$\mathrm{Prob}\,(x_i \leq x) = P(x) = \int_{-\infty}^{x} p(v)\,\mathrm{d}v \tag{2.2}$$

This inherent randomness ensures that two realizations of the breaking of a fibre bundle will not be identical, and the study of fibre bundle models thus has a statistical nature. Many samples are needed, both when studying fluctuations and averages. An example of this is shown in Fig. 2.2, where the strain curve, described in the next paragraph, from a single sample is compared to the same quantity averaged over many samples, both of them in one dimension and with local load sharing. The former fluctuates a lot and is highly dependent on the sample in question, i.e. the N thresholds drawn from $p(x)$, while the latter is a quantity that could be compared to relevant analytical results if they exist.

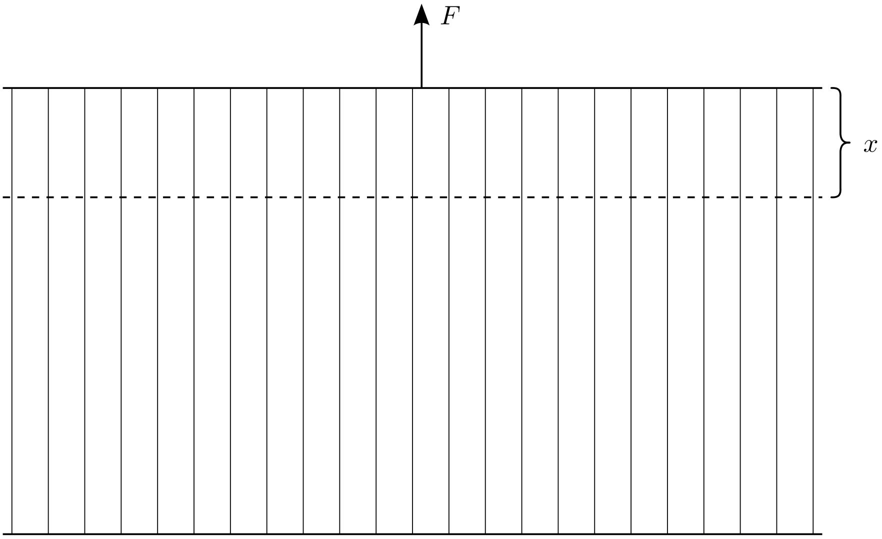

Figure 2.1: Illustration of a one-dimensional equal load sharing fibre bundle. The fibres are fastened between two infinitely stiff clamps, forming a bundle. When exposed to an external force F, the fibres are stretched from their original positions – shown with a dashed line – by a distance x.

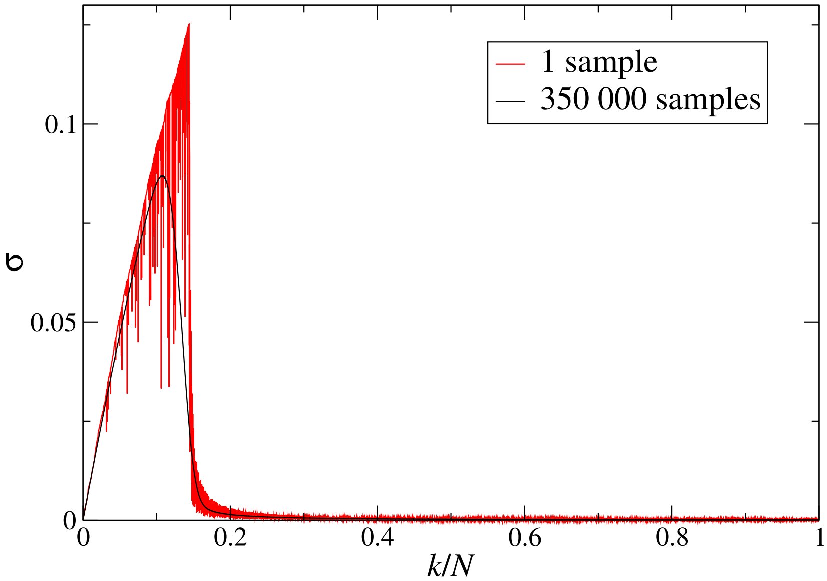

Figure 2.2: The strain curve for a fibre bundle of size $N = 10^4$ with local load sharing in one dimension when $P(x) = x$. The red curve shows a single sample while the black curve is averaged over $3.5 \cdot 10^5$ samples.

2.1.2 Strain curve

When the fibre bundle is affected by a force F and has k broken fibres, the force per fibre is defined as $\sigma = F/N$. Note that this is not the force per remaining fibre, $N - k$, but per the total number of fibres, to make it comparable between different places in the breaking process, i.e. for different values of k. As mentioned earlier, Fig. 2.2 shows the *strain curve*, the least force per fibre σ required to break the next fibre as a function of the fraction of broken fibres k/N, both for a single sample and averaged over many samples.

When loading a fibre bundle, one can proceed in two different ways. In the first, the force acting on the bundle is increased in steps, and in each step any fibres too weak to support the increased load are broken. This is done until the entire bundle breaks down. It is clear that in each step, the number of fibres breaking are going to vary; sometimes none will break and sometimes many will break at the same time. This method is called the force controlled method because the force applied on the fibre bundle is the control parameter.

In the second, the strain controlled method, the strain, i.e. the extension of the bundle, is the control parameter. It is increased from zero until a single fibre breaks, and then it is once again set to zero. This is then repeated N times until every fibre has been broken. Such an experiment yields the previously mentioned strain curve, so named because of its origin from this method of breaking a fibre bundle.

2.1.3 Burst size distribution

The *burst size distribution* $D(\Delta)$, which can also be called the exclusive burst size distribution to distinguish it from the distribution of inclusive bursts [11], is related to the force controlled method of breaking fibre bundles; when Δ fibres fail simultaneously it is called a burst of size Δ, and $D(\Delta)$ is the expected number of bursts of size Δ that occur during the breaking of the entire fibre bundle.

In terms of the strain curve, one can define a burst of size Δ beginning when breaking fibre number k_0 via two conditions. Firstly, the force used when initiating the burst must be higher than the force required for breaking any previous fibres. Let σ_k be the force per fibre required to break fibre number k in the bundle. Then the first condition can be written mathematically as $\sigma_{k_0} > \sigma_k \ \forall \ k < k_0$, which corresponds to the fact that the burst must begin when breaking fibre number k_0. If any of the previous forces were higher, the burst would have begun there in a force controlled experiment.

Secondly, the next $\Delta - 1$ fibres must break at a lower force than k_0 did, and $k_0 + \Delta$ must require a higher force to break to stop the burst. This can be formulated as $\sigma_{k_0} \geq \sigma_{k_0+j}$ for $j = 1, 2, 3, \ldots, \Delta - 1$ and $\sigma_{k_0} < \sigma_{k_0+\Delta}$ via the strain curve. Then exactly Δ fibres fail simultaneously once the force reaches σ_{k_0}, and a burst of size Δ occurs.

How the burst size distribution $D(\Delta)$ acts as a function of the burst size Δ depends on both the force distribution of the fibre bundle model, the bundle size N and the threshold distribution $P(x)$, as we will see later when we discuss equal and local load sharing.

2.1.4 Dimensionality

We refer to Fig. 2.1 for an illustration of how the fibre bundle looks in one dimension. The N fibres are arranged on a line, and periodic boundary conditions are used so that every fibre has two nearest neighbours. Defining a *hole* as a collection of connected, broken fibres – in the sense that two fibres are connected if they are nearest neighbours – and its *perimeter* as the unbroken fibres that have nearest neighbours included in the hole, we see that any hole in the one-dimensional model has a perimeter consisting of only two fibres, independent of the size of the hole. (There is one exception, namely when there is only one unbroken fibre left, and there is a single large hole of size $N-1$ with the last surviving fibre as its perimeter.) The notion of a hole and its corresponding perimeter will become important when generalizing the local load sharing model to higher dimensions in Section 2.3.4.

When generalizing to higher dimensions we place the fibres in a hypercubic pattern, also here using periodic boundary conditions. Thus, in D dimensions, any fibre has $2D$ nearest neighbours and the total number of fibres can be written $N = n^D$, where n is some positive integer. It is worth noting that the two-dimensional model corresponds to a physical system in three dimensions, while the models with $D \geq 3$ seemingly do not describe any realizable physical systems.

2.2 Equal load sharing

The equal load sharing (ELS) – also called global load sharing – model is the oldest and simplest of the fibre bundle models, in which force is distributed equally among the intact fibres at all times. Due to the simplicity of the model, it is possible to derive a number of analytical results about it, as shown by for instance Daniels in 1945 [12].

2.2.1 Force distribution

A rationalization of equal load sharing can be seen from Fig. 2.1. There the clamps connected by the fibres are infinitely stiff, meaning that any fibre is stretched equally far, and thus they all carry the same load since the elastic constant is identical for all fibres.

When k fibres have failed the force acting on the bundle is evenly distributed among the $N-k$ remaining fibres. The extension x of the bundle is then given by

$$\sigma = \kappa \left(1 - \frac{k}{N}\right) x \tag{2.3}$$

meaning that for a given force per fibre σ the fibres are stretched further when more have failed, since the total force is distributed on fewer fibres.

2.2.2 Strain curve

From Eq. (2.3) and the definition of the strain curve, it is clear that the strain curve for equal load sharing is given by the relation

$$\sigma = \kappa \left(1 - \frac{k}{N}\right) \cdot \min_{i \in \Omega} (x_i) \tag{2.4}$$

between σ and k, where Ω is the set of numbers corresponding to the remaining fibres. If the fibres are numbered from weakest to strongest, i.e. $x_1 \leq x_2 \leq \ldots \leq x_{N-1} \leq x_N$, then $\Omega = \{k+1, k+2, \ldots, N-1, N\}$ and $\min_{i \in \Omega} (x_i) = x_{k+1}$, giving

$$\sigma = \kappa \left(1 - \frac{k}{N}\right) x_{k+1} \tag{2.5}$$

when breaking fibre number $k+1$.

Exactly how this curve looks depends on the threshold distribution $P(x)$, but the resulting formulas can be derived via order statistics [13]. With $P(x) = (x - x_<) / (1 - x_<)$, the uniform distribution on $(x_<, 1)$, the result is the formula

$$\sigma = \kappa \left(1 - \frac{k}{N}\right) \left(x_< + (1 - x_<) \frac{k}{N}\right). \tag{2.6}$$

When $x_< = 0$, meaning that $P(x)$ is the uniform distribution on the unit interval, this becomes the simple parabola

$$\sigma = \kappa \left(1 - \frac{k}{N}\right) \frac{k}{N}. \tag{2.7}$$

The distribution $P(x) = 1 - \exp(-x + x_<)$, where $x \in [x_<, \infty)$, on the other hand, yields

$$\sigma = \kappa \left(1 - \frac{k}{N}\right) \left(x_< - \ln\left(1 - \frac{k}{N}\right)\right). \tag{2.8}$$

The derivation of these results requires taking the limit $N \to \infty$, so they are only accurate for large bundles.

2.2.3 Burst size distribution

Hemmer and Hansen [11] have shown that with equal load sharing the burst size distribution is a power law

$$\frac{D(\Delta)}{N} \propto \Delta^{-\xi} \tag{2.9}$$

with an exponent $\xi = \frac{5}{2}$ for a large class of threshold distributions, including $P(x) = x$ and $P(x) = 1 - \exp(x_< - x)$. The result is valid for large bundles, $N \to \infty$, and for large Δ, as the Stirling approximation, $\Delta! \simeq \sqrt{2\pi\Delta}\Delta^{\Delta}\mathrm{e}^{-\Delta}$, is used in the derivation.

2.2.4 Higher dimensions

Since the ELS force distribution does not depend on the placement of fibres, in particular which fibres are neighbours of each other, but only on the number of broken fibres, the ELS model will be independent of which dimension we use. One *can*, of course, arrange the fibres in a D-dimensional hypercube with $D > 1$, but the breaking process will – given the same set of thresholds $\{x_i\}$ – proceed in exactly the same way as in one dimension. That is, the fibres will break in the same order and at the same applied force. Hence one can talk about the ELS model without specifying the dimension, as it behaves identically in all dimensions.

2.3 Local load sharing

The one-dimensional local load sharing (LLS) model as we will use it was first introduced by Harlow and Phoenix in 1978 with the intention of creating a more realistic fibre bundle model for composite materials [14]. In local load sharing, all force from broken fibres is transferred onto the nearest neighbours.

While the ELS fibre bundle model is extreme in the sense that force is equally distributed among fibres no matter the state of the bundle, the LLS model is extreme in the opposite way: the force originally carried by a fibre that breaks is divided between its nearest neighbours only. Any other physically reasonable way of distributing the force will be somewhere in between these two extremes. Examples of this are the soft clamp model [15] and the γ-model of Hidalgo et al. [16].

2.3.1 Force distribution

We use the same force distribution in one dimension as Harlow and Phoenix originally did [14], with the force f_i on fibre number i being given by

$$f_i = \left(1 + \frac{r_i}{2}\right)\sigma \tag{2.10}$$

for intact fibres; broken fibres carry no force at all. Here σ is once again the force per fibre F/N and r_i is the sum of consecutive failed fibres immediately to the left and to the right of fibre number i. This distribution is history independent as the force acting on each fibre is determined solely from the state of the bundle – i.e. which fibres are broken – at the time of loading.

With this way of distributing forces it is easily seen that the sum of the loads on all fibres is $N\sigma = F$, which must be required for the model to be self-consistent. Note that this also applies when there is only one intact fibre left, since $r_i = 2(N-1)$ for the remaining fibre because of the periodic boundary conditions; when counting consecutive broken fibres both to the left and the right, all the $N-1$ broken fibres are counted twice.

While Eq. (2.10) should leave no doubt as to how force is distributed among the fibres, a description with words is often more ambiguous. "The extreme form for local load redistribution is that all extra stresses caused by a fiber failure are taken up by the *nearest-neighbor* surviving fibers. . . . In this case precisely two fibers, one on each side, take up, and divide equally, the extra stress.", as said in Ref. [17], could be interpreted as simply dividing the force acting on a fibre between its two nearest neighbours once it fails. This, however, leads to a history dependence as seen in Fig. 2.3; the force distribution would depend not only on the configuration of failed fibres, but also on the order in which they break. This is not physically acceptable, but despite this, many have implemented the local load sharing model this way numerically, which is why we stress that we use a history-independent force distribution.

2.3.2 Strain curve

From Eq. (2.1) and (2.10) it is clear that the strain curve for local load sharing in one dimension is given by

$$\sigma = \min_{i\in\Omega}\left(\frac{\kappa x_i}{1 + \frac{r_i}{2}}\right) \tag{2.11}$$

where Ω again is the set of numbers corresponding to the surviving fibres. The dependence on the number of broken fibres k is hidden in r_i, which will depend on k in some way.

Unlike ELS, where we could easily evaluate the minimum by renumbering the fibres, there is no easy way to simplify this expression. We will not attempt to do any simplifications or analytical evaluations for different probability distributions, but an example

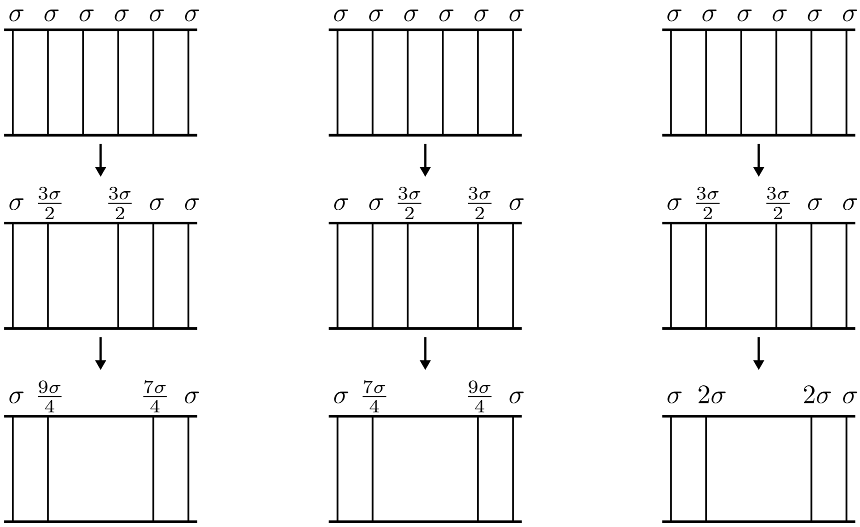

Figure 2.3: How local load sharing is implemented in one dimension when fibres break. The two leftmost columns show a history-dependent distribution rule where the force from a failing fibre is divided equally between its nearest neighbours in each direction. The right column shows how we implement it, via Eq. (2.10). For simplicity the additional elongation of fibres under higher loads is not shown.

of this curve, computed numerically, is shown in Fig. 2.2 with the threshold distribution uniform on the unit interval, $P(x) = x$.

2.3.3 Burst size distribution

It has been shown by Kloster, Hansen and Hemmer [17] that it is possible to calculate the burst size distribution for local load sharing in one dimension analytically with a uniform threshold distribution, although it is very complicated. They found that with a bundle size $N = 20\ 000$ the burst size distribution follows a power law $D(\Delta) \propto \Delta^{-5}$ for very small Δ. This power law quickly veers off into an exponential decay as Δ increases, making the power law description valid only for Δ smaller than roughly 10.

Considering several other distributions as well, Zhang and Ding [18] found that for small Δ there is a power law dependence

$$D(\Delta) \propto \Delta^{-\xi}, \tag{2.12}$$

but the exponent ξ depends on the threshold distribution and increases with increasing bundle size.

In the article that sparked the investigation of Zhang and Ding, Hansen and Hemmer [19] showed numerically that with a uniform threshold distribution and $N = 5000$, there is a power law dependence as in Eq. (2.12) with $\xi \simeq 4.5$.

2.3.4 Generalization to higher dimensions

When generalizing the LLS fibre bundle model to higher dimensions, we insist on keeping it history independent like it was in one dimension. Using the definitions of a hole and its perimeter from Section 2.1.4, and using h_j for the number of fibres in hole number j as well as s_j for the number of fibres in the perimeter of the same hole, we let the force on a surviving fibre be

$$f = \left(1 + \sum_j \frac{h_j}{s_j}\right)\sigma, \tag{2.13}$$

where the sum is over the different holes the fibre in question is in the perimeter of - i.e. is a neighbour of.

It is easy to verify that the sum of this force over all fibres gives a total of $N\sigma = F$, as it should. When specializing to one dimension s_j will be two, except for the case when there is only one intact fibre left, when it is one. This reproduces Eq. (2.10), which is required to make Eq. (2.13) a proper generalization.

The dependence on dimension in Eq. (2.13) is contained in the relation between h_j and s_j. As an example, when $h_j = 1$ then $s_j = 2D$ in D dimensions, increasing linearly with the dimension.

For a given bundle size, it is easily discernible that the LLS model will become more similar to the ELS model as the dimension increases. Any fibre will have more nearest neighbours in a higher dimension, and thus a hole of a given size will on average have a larger perimeter, distributing the forces more evenly across the fibre bundle and hence acting more like the ELS model.

3 Algorithms and simulations

This chapter details the algorithms used and a few specifics about the simulations. Section 3.1 describes how holes and their perimeters are found, with Section 3.1.1 containing the algorithm used for grouping failed fibres together in holes, and Section 3.2 gives a short description of the simulations we have done, including a mention of how parallelization is handled.

3.1 Finding holes and perimeters

To calculate the force distribution in local load sharing, it is necessary to have a list of existing holes plus knowledge of how large they are and what fibres are in their perimeters, as seen from Eq. (2.13). To do this effectively we employ a variation of the Hoshen-Kopelman algorithm [20], a special case of the more general union find algorithms, which are used to group objects into disjoint sets based on an equivalence relation defined on the objects. See for instance *Introduction to Algorithms* [21] for more detailed information about the union find algorithms.

3.1.1 Determining hole structure

First number the N fibres with a label $i \in \{1, 2, 3, \ldots, N-1, N\}$ and then make use of an array $T = [t_1, t_2, \ldots, t_i, \ldots, t_N]$. The array represents a function $f : \Phi \to \Phi$ from the set of all fibres $\Phi = \{1, 2, \ldots, N-1, N\}$ onto itself, where $f(i) = t_i$. Initially $f(i) = t_i = i$, so f is the identity function.

Throughout the process of identifying holes a single fibre in each hole is chosen to represent the entire hole. This choice is entirely arbitrary, and for simplicity we will use the fibre with the lowest label of those included in the hole. Once the algorithm has been executed, T will contain references from broken fibres to the fibre representing the hole it is a part of, i.e. t_i will be the label of the fibre representing the hole fibre number i is included in. Since $t_i = i$ to begin with, every broken fibre is considered a separate hole and is its own representative at the beginning of the algorithm.

Then define a positive and negative direction for each dimension in the D-dimensional hypercube, meaning that any fibre has D neighbours when counting only in the positive directions. Looping over all of the N fibres, consider the neighbours in positive directions only. As illustrated in Fig. 3.1 for two dimensions, this covers all neighbour relations between the fibres exactly once, including the ones emerging from the periodic boundary conditions. Neighbours in negative directions are not considered to avoid covering the same neighbour relations twice.

Doing this loop over all fibres, first check if the fibre in question, labelled i, is broken. If it is, then check whether its neighbours in the positive directions are broken as well. In addition, define the sequence $b_{i,l}$ via $b_{i,0} = t_i$ and $b_{i,l+1} = f\left(b_{i,l}\right) = t_{b_{i,l}}$ and iterate until $b_{i,m+1} = b_{i,m}$ for some m. Then $b_{i,m}$ is the representative of the hole i is a member of.

If a neighbour, labelled j, is also broken it is part of the same hole as i. Similarly define the sequence $c_{j,l}$ via $c_{j,0} = t_j$ and $c_{j,l+1} = f\left(c_{j,l}\right) = t_{c_{j,l}}$ and iterate until $c_{j,h+1} = c_{j,h}$ for some h, so that $c_{j,h}$ is the representative of the hole j is a part of.

Since the two fibres i and j are in the same hole, so are their representatives $b_{i,m}$ and $c_{j,h}$, and so we let $t_a = \min\left(b_{i,m}, c_{j,h}\right)$, with $a = \max\left(b_{i,m}, c_{j,h}\right)$, letting $\min\left(b_{i,m}, c_{j,h}\right)$

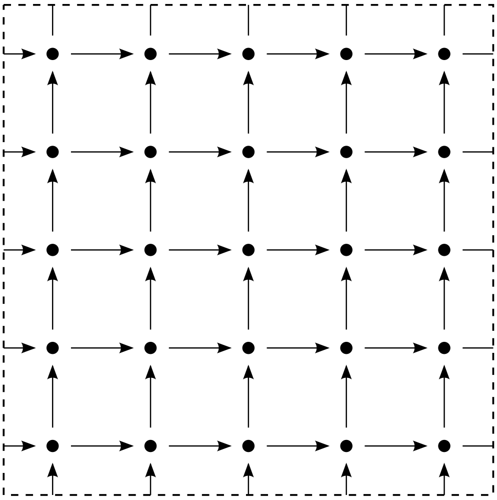

Figure 3.1: Illustration of neighbour relations – arrows indicate positive directions – for a two-dimensional fibre bundle of size $N = 25$. The fibres are shown as black discs and the dashed lines are where we apply periodic boundary conditions.

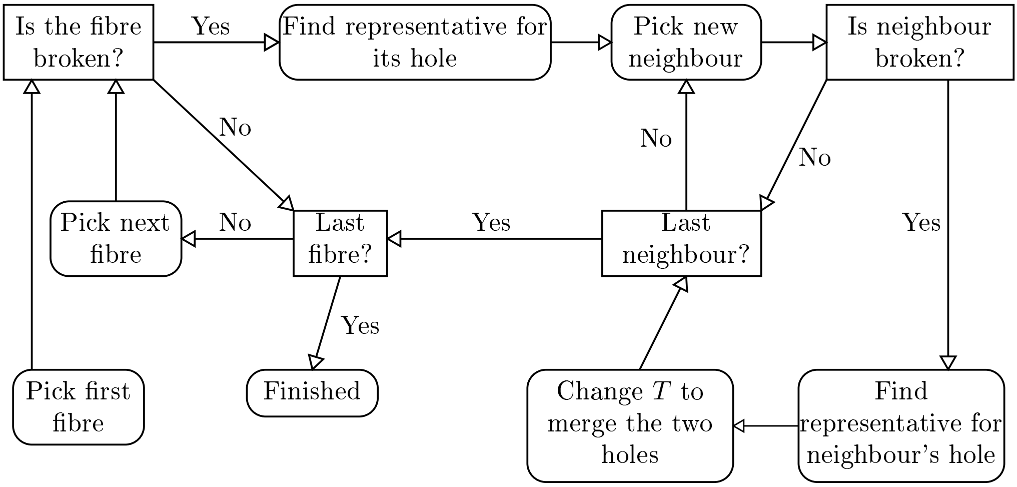
Is the fibre broken?
Yes
Find representative for its hole
Pick new neighbour
Is neighbour broken?
No
No
No
Pick next fibre
No
Last fibre?
Yes
Last neighbour?
Yes
Yes
Pick first fibre
Finished
Change T to merge the two holes
Find representative for neighbour's hole

Figure 3.2: Flowchart of the algorithm to determine which fibres are part of the same holes. Only neighbours in positive directions are considered.

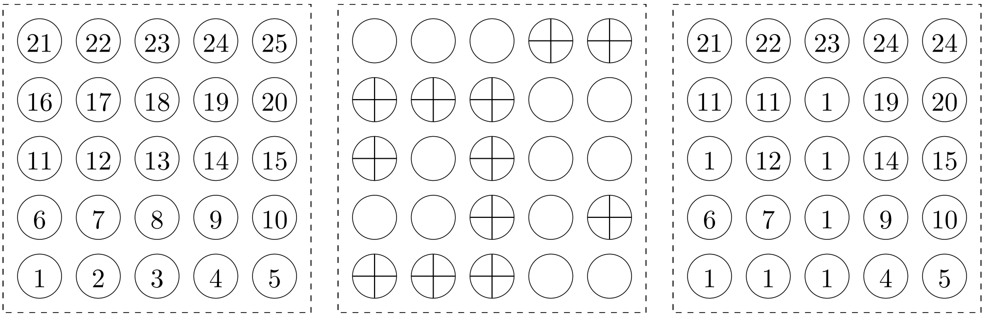

(a) Fibre numbering (b) Bundle state (c) T

Figure 3.3: An example in two dimensions with $N = 25$. Fibre numbering is shown in (a) and (b) displays the bundle state with intact fibres as open circles and broken fibres as crossed ones. (c) shows the values t_i for the bundle after using the algorithm from Fig. 3.2 with the positive directions from Fig. 3.1.

represent the new and larger hole. As $b_{i,m}$ and $c_{j,h}$ were the smallest labels in their respective holes, this is consistent with letting the fibre with smallest label represent its hole.

Once all neighbours in positive directions have been checked, go on to the next fibre and repeat the procedure above. The entire process is outlined as a flowchart in Fig. 3.2.

When this algorithm is finished, all fibres in the same hole are connected to a single fibre representing that hole, but as illustrated by the example in Fig. 3.3c we are not guaranteed that t_i for all these fibres will point *directly* to the representative. To ensure this, loop over all fibres and once again use the sequence $b_{i,l}$ as defined earlier. Iterate until $b_{i,m+1} = b_{i,m}$ for some m, as before, and then let $t_i = b_{i,m}$ since $b_{i,m}$ is the representative of the hole i is in. Now all broken fibres i point to their hole's representative via t_i.

3.1.2 Perimeters and hole sizes

When the hole structure has been found it is easy to find hole sizes and perimeters. Loop over all fibres, initially setting all hole sizes to zero and letting all perimeters be empty. If the fibre is broken, add one to the size of its hole. If it is not, then check which holes, if any, it is a neighbour of. When the loop is complete, we have knowledge of the sizes of all holes and which fibres are in their perimeters, which is all we need to calculate the LLS force distribution.

3.1.3 Comments

It is worth mentioning how the speed of the union find algorithm described in Section 3.1.1 scales with the dimension of the fibre bundle we simulate. The way we have implemented it, the number of operations required by the algorithm scales as $N \ln N$ with the number of fibres N [21]. This, however, says nothing about what happens when we compare two bundles of equal size, i.e. the same N, but with different dimensions. When the dimension increases, so does the number of neighbours for each fibre, even when only those in the defined positive directions are included. Because of this, the innermost part of the algorithm – looping over neighbours in positive directions – will consist of more operations, meaning that the speed of the algorithm decreases when the dimension increases. For any given dimension the number of operations still scales as $N \ln N$, but the proportionality constant will increase with the dimension.

For this reason, we average over fewer samples for higher dimensions when using roughly the same bundle size, as the number of samples one can compute within a reasonable amount of time is lower than for a lower dimension. The bundle sizes, dimensions and number of samples used in the simulations are given for all the results presented in Section 4.

The entire process explained in the previous two sections is repeated for each time a fibre is broken to find the new hole structure after the fibre has failed. While the union find algorithms are very fast, there is more information available that is not used by this procedure. When doing a strain controlled breaking of a fibre bundle from beginning to end, which fibres have already failed and how the hole structure looked before breaking the next fibre is also known; the algorithm is not given random bundle states at any step.

Taking this into account, it might be possible to make a faster algorithm by, for each fibre broken, modifying the hole structure from the previous state, which the current algorithm does not use at all. Doing this is reported to have significantly sped up the numerics of the two-dimensional LLS model [22].

3.2 Simulations

We have done simulations of strain-controlled breaking of fibre bundles with both the ELS and LLS models for a few different threshold distributions and bundle sizes in up to five dimensions, using dimensionless units and $\kappa = 1$. Unlike a physical strain-controlled experiment, where it would be necessary to increase the strain infinitesimally until a fibre breaks before setting it to zero again, we can simply find the fibre that breaks under the lowest external load since the thresholds of all the fibres are known during the simulation.

3.2.1 Parallelization

The algorithm explained in Section 3.1 takes up a very large part of the time used when computing local load sharing, but it is not possible to parallelize it. However, since getting useful results requires computing many samples, it is easy to avoid this problem and parallelize the program by making different threads compute different samples. This is what we have done in our simulations.

4 Results

In this chapter we present the results of the simulations carried out using the models from Chapter 2. First results from one dimension are presented in Section 4.1, for comparison to existing results in the discussion. We then look at the strain curves, with Section 4.2 displaying size dependencies in four dimensions with $P(x) = x$ and Section 4.3 showing dimensional dependencies. Lastly, Section 4.4 displays the LLS burst size distribution in two to five dimensions.

4.1 One dimension

We first present the results from simulations of equal and local load sharing in one dimension. The main reason for singling out one dimension is that the existing literature on the fibre bundle models that is directly comparable to our results only considers one dimension, and hence only this dimension is suitable for comparing results and establishing whether the model has been implemented correctly.

4.1.1 Strain curves

To begin with we show numerical results for strain curves, both for the ELS and LLS fibre bundle model, in one dimension.

Equal load sharing
The analytical ELS strain curve with $P(x) = x$, Eq. (2.7), is compared to the strain curves from simulations with the same threshold distribution, showing the difference in Fig. 4.1. Two different bundle sizes are used, $N = 10^4$ and $N = 10^5$, whose data sets are averaged over $3.5 \cdot 10^5$ and $2 \cdot 10^4$ samples, respectively.

The simulations are seen to differ little from the analytical, large-N result, with better overall similarity for the largest bundle. We also observe that it seems as though finite size effects affect the difference the most when k/N is close to one, and note that the difference goes to $1/N$ as $k/N \to 1$ for these two bundle sizes.

For the distribution $P(x) = 1 - \exp\left(-x + x_<\right)$, Fig. 4.2 displays the difference between ELS strain curves from simulations and the analytical result, Eq. (2.8), both for $x_< = 0$ and $x_< = 1$. The simulations used $N = 10^4$ and $3.5 \cdot 10^5$ samples for averaging.

This shows a good correspondence between the simulations and the analytical result, and finite size effects seem to mostly occur for the larger values of k, like for the uniform distribution. Curiously, the difference for $x_< = 1$ does not go to zero once k/N gets small enough, like the other distributions, but goes to $1/N$ instead.

Local load sharing
The strain curves for local load sharing in one dimension is shown in Fig. 4.3 for three different threshold distributions: $P(x) = x$ and $P(x) = 1 - \exp\left(-x + x_<\right)$ with $x_< = 0$ and $x_< = 1$. For all three distributions the bundle size is $N = 10^4$ and the results are averaged over $3.5 \cdot 10^5$ samples.

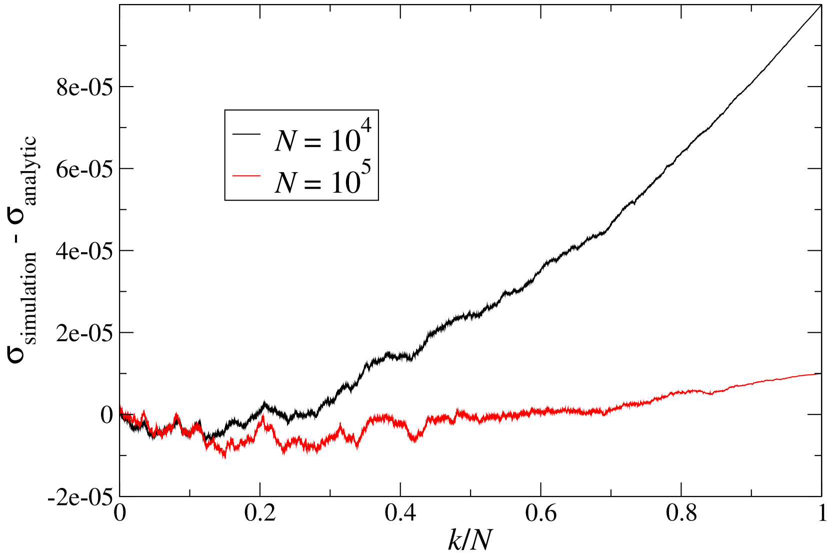

Figure 4.1: Difference between ELS strain curves from simulations and analytical results when $P(x) = x$ for two different bundle sizes: $N = 10^4$ (black) and $N = 10^5$ (red).

4.1.2 Burst size distribution

This section contains results for the burst size distribution with $P(x) = x$ both for equal and local load sharing in one dimension.

Equal load sharing

The burst size distribution with ELS for two bundles with sizes $N = 10^4$ and $N = 10^5$ is shown in Fig. 4.4, using $3.5 \cdot 10^5$ and $2 \cdot 10^4$ samples, respectively.

For small enough Δ there is a clear power law dependence, and fitting a power law to $D(\Delta)$ for $\Delta \leq 8$ gives an exponent of $\xi \simeq 2.71$ for $N = 10^4$ and $\xi \simeq 2.72$ for $N = 10^5$. This is not especially close to the theoretical value of $\xi = 2.5$ from Eq. (2.9), but these values will be useful for a comparison to the burst size distribution for local load sharing.

However, since the universal exponent is valid only for large Δ, we also try to fit a power law to the burst size distribution when the smallest bursts, for which the Stirling approximation is not that good, are removed. Fig. 4.5 shows the burst size distributions from Fig. 4.4 with $50 \leq \Delta \leq 200$ and corresponding power law fits. They give exponents of approximately $\xi \simeq 2.54$ $(N = 10^4)$ and $\xi \simeq 2.49$ $(N = 10^5)$.

In Fig. 4.4 one can also see spikes in $D(\Delta)$ for $\Delta \approx N/2$, which corresponds to the fatal bursts that break the entire fibre bundle and begin close to the maximum of the strain curve, at $k/N = 0.5$.

Local load sharing

The burst size distribution for a one-dimensional LLS bundle of size $N = 10^4$, calculated from $3.5 \cdot 10^5$ samples, is shown in Fig. 4.6.

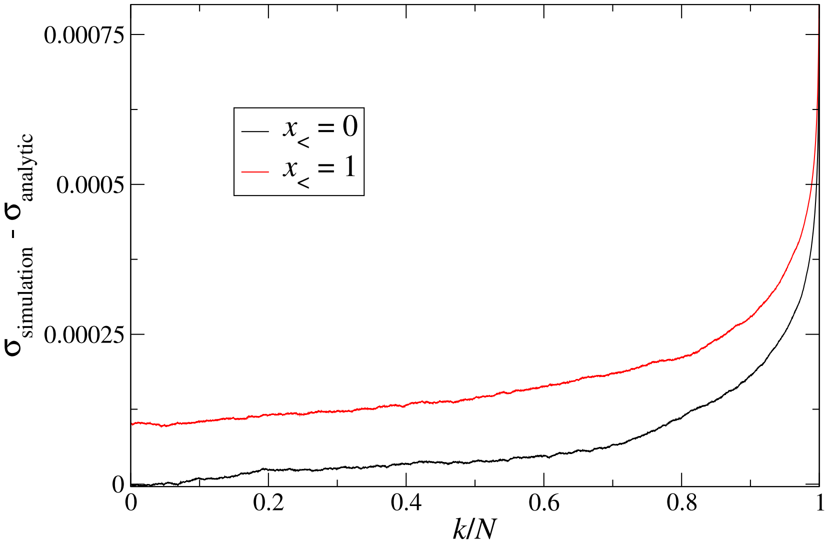

Figure 4.2: Difference between ELS strain curves from simulations and analytical results when $P(x) = 1 - \exp(-x + x_<)$ for $x_< = 0$ (black) and $x_< = 1$ (red).

A power law fit to the distribution for the eight lowest values of Δ gives an exponent (see Eq. (2.12)) of $\xi \approx 4.6$. Also, there is a spike situated at $\Delta \approx 0.88N$ that signifies the fatal bursts where the fibre bundle breaks down.

4.2 Size dependence in four dimensions

This section showcases the size dependency of the difference between the strain curve for LLS and ELS in four dimensions. There are two possible ways of doing this, using either analytical results for ELS or using results from actual simulations. In the following we look at size dependences for both of these with the threshold distribution uniform on the unit interval, $P(x) = x$ with $x \in (0, 1)$.

4.2.1 Analytical ELS results

In this section the analytical result for the ELS strain curve with the uniform distribution on the unit interval, i.e. Eq. (2.7), is used. Using this to define σ_{ELS} and letting σ_{LLS} be the averaged strain curves from LLS simulations, the difference between these two for five bundle sizes – $N = 4^4$, 6^4, 8^4, 10^4 and 12^4 – in four dimensions is shown in Fig. 4.7. The results are averaged over $5 \cdot 10^5$, $2.5 \cdot 10^5$, $2.5 \cdot 10^5$, $4 \cdot 10^4$ and $2 \cdot 10^4$ samples, respectively.

Finite size effects are seen to appear mostly for larger values of k/N, like for equal load sharing in Section 4.1.1, changing the difference significantly for the smaller bundles compared to the larger ones.

As we will see later, from for instance Fig. 4.13, the maxima of this difference moves when the dimension changes. Hence, to evaluate how big the difference between ELS and

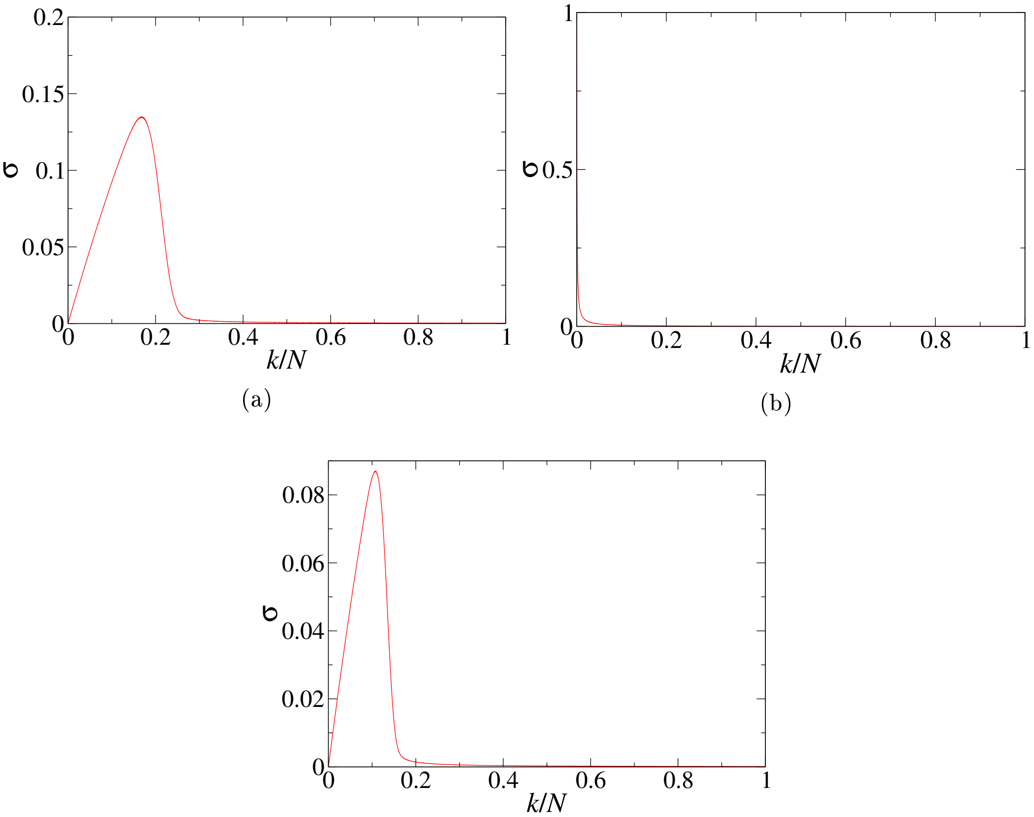

(a)

(b)

(c)

Figure 4.3: Averaged strain curves for LLS in one dimension for three different threshold distributions: $P(x) = 1 - \exp(-x)$ (a), $P(x) = 1 - \exp(-x + 1)$ (b) and $P(x) = x$ (c).

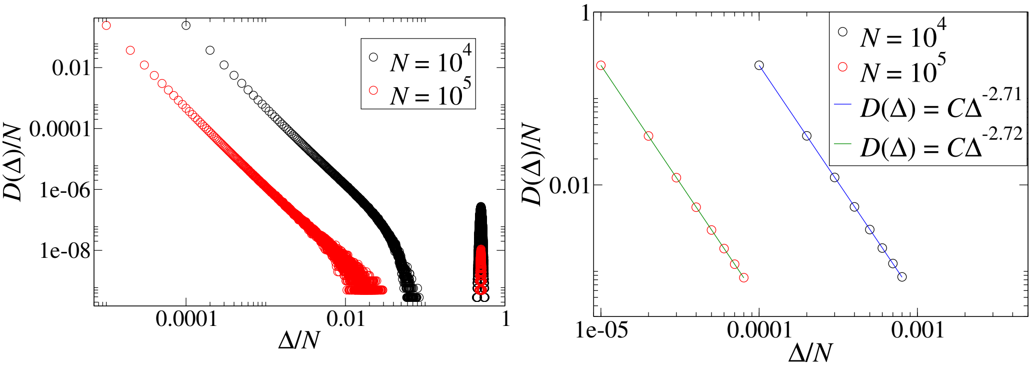

(a)

(b)

Figure 4.4: Burst size distributions for two ELS bundles with sizes $N = 10^4$ (black) and $N = 10^5$ (red). (a) shows the entire distribution while (b) shows only $\Delta \leq 8$ together with corresponding power law fits.

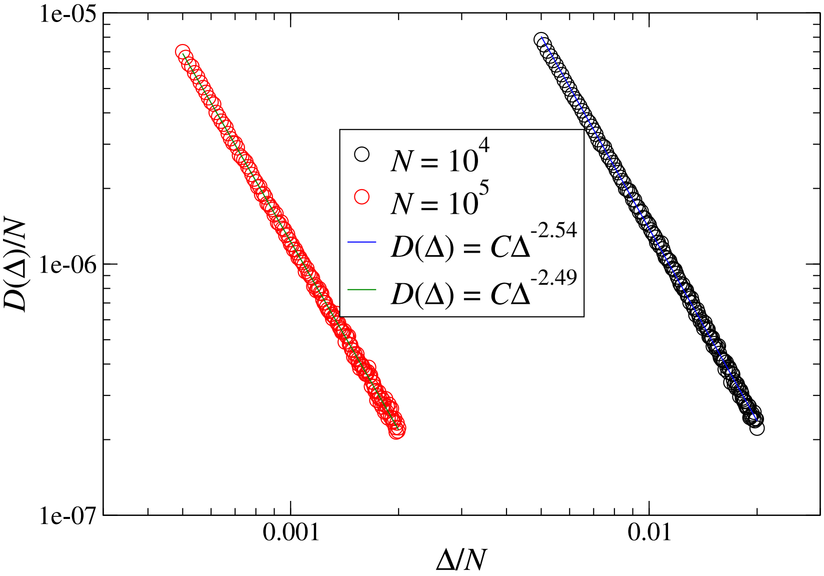

Figure 4.5: ELS burst size distribution when $50 \leq \Delta \leq 200$ for $N = 10^4$ (black) and $N = 10^5$ (red) with corresponding power law fits.

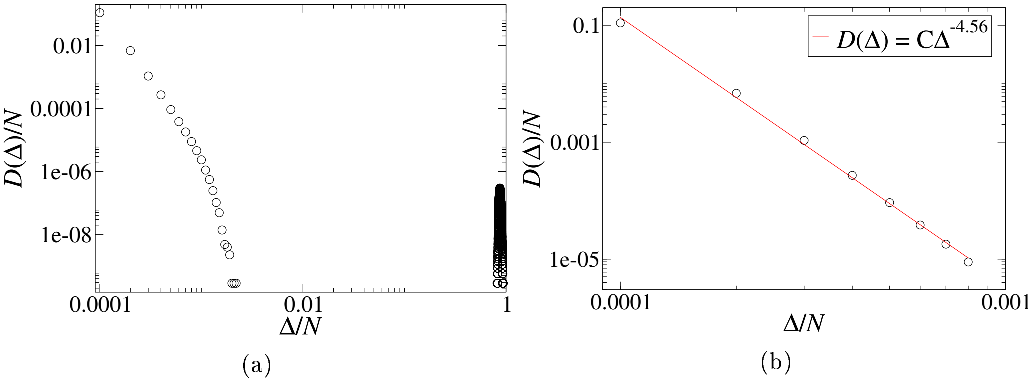

(a) (b)

Figure 4.6: LLS burst size distribution for a one-dimensional bundle of size $N = 10^4$. The entire distribution is shown in (a) while (b) shows $\Delta \leq 8$ and a corresponding power law fit.

LLS is, we must calculate a total difference of some kind. We propose two ways of doing this, using

$$\Delta\sigma_1 = \frac{1}{N}\sum_k |\sigma_{\mathrm{ELS}}(k) - \sigma_{\mathrm{LLS}}(k)| \tag{4.1}$$

and

$$\Delta\sigma_2 = \frac{1}{N}\sum_k (\sigma_{\mathrm{ELS}}(k) - \sigma_{\mathrm{LLS}}(k)) \,. \tag{4.2}$$

The latter method is the average over all the data points in the curve $\sigma_{\mathrm{ELS}} - \sigma_{\mathrm{LLS}}$, which in the limit $N \to \infty$ corresponds to the Riemann sum expression for the integral, while the former is an average of the absolute value of the data points.

Using these two definitions on the strain curves from Fig. 4.7, we get Fig. 4.8 that shows these total differences as functions of $1/N$. From the figure it looks like both the two measures seem to converge to roughly the same value when $N \to \infty$. See Table 4.1 for the values for the two largest bundles. Doing a linear fit to $\Delta\sigma_1$ as a function of $1/N$ yields $\Delta\sigma_1 = 0.189/N + 0.001353$, indicating that $\Delta\sigma_1 \to 0.001353$ as N goes to infinity.

We also notice that, although there is a huge discrepancy between $\Delta\sigma_1$ and $\Delta\sigma_2$ for the smaller bundles, the two largest bundles have similar $\Delta\sigma$-values regardless of the method used. These values are shown in Table 4.1. They are only a few percent off from one another, and in addition they are also only a few percent off from our estimate of $\Delta\sigma_1$ as $N \to \infty$.

4.2.2 Numerical ELS results

Since Eq. (2.7), the analytical result for the ELS strain curve, is only valid in the large-N limit, it seems reasonable to use results from ELS simulations when studying size dependency. This eliminates errors stemming from discrepancies between the analytical ELS result and actual ELS simulations for finite bundle sizes.

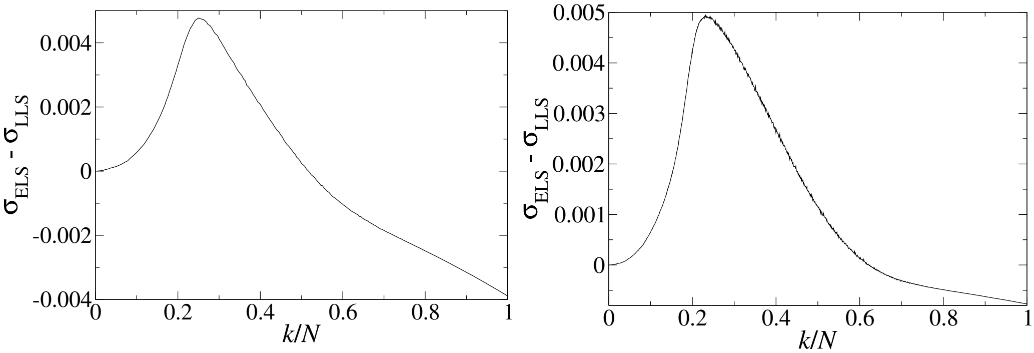

(a) $N = 4^4$ (b) $N = 6^4$

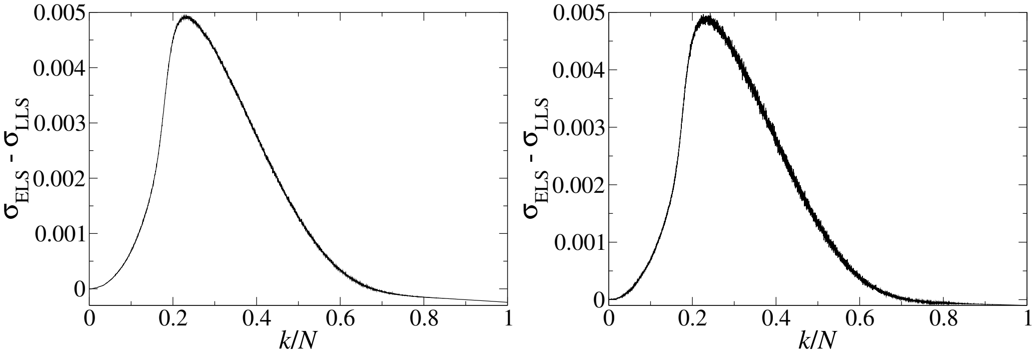

(c) $N = 8^4$ (d) $N = 10^4$

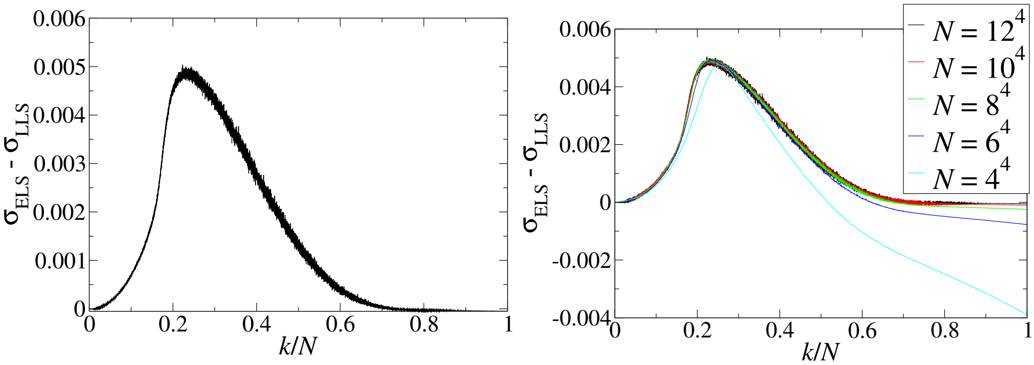

(e) $N = 12^4$ (f) A comparison.

Figure 4.7: The difference between LLS and analytical ELS strain curves, $\sigma_{\text{ELS}} - \sigma_{\text{LLS}}$, in four dimensions with $P(x) = x$. Subfigures (a)-(e) show different bundle sizes while Subfigure (f) shows a comparison of (a)-(e).

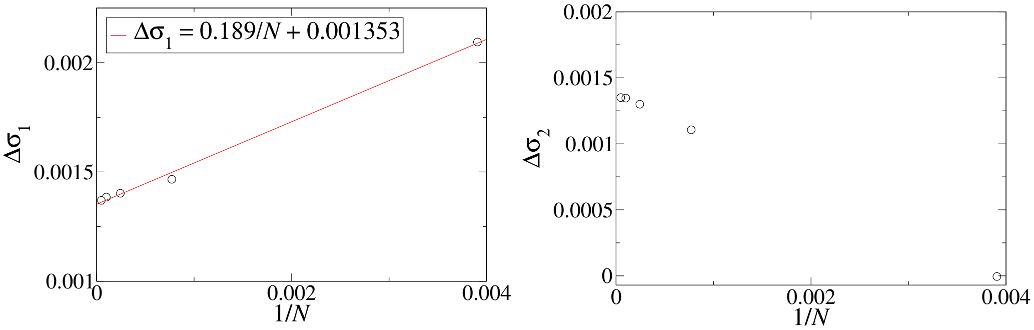

(a) $\Delta\sigma_1$ for the curves in Fig. 4.7.

(b) $\Delta\sigma_2$ for the curves in Fig. 4.7.

Figure 4.8: $\Delta\sigma_1$ (a) and $\Delta\sigma_2$ (b) for $P(x) = x$ in four dimensions as functions of $1/N$ when using the analytical ELS strain curve, Eq. (2.7). In (a), the red line is a linear fit to the data points.

Table 4.1: $\Delta\sigma_i$-values for the two largest bundles both when using ELS strain curves from simulations and the analytical result.

	Analytical ELS	ELS from simulations
$\Delta\sigma_1$ $(N = 10^4)$	0.001385002	0.001390294
$\Delta\sigma_2$ $(N = 10^4)$	0.001346383	0.001390294
$\Delta\sigma_1$ $(N = 12^4)$	0.001370013	0.001373112
$\Delta\sigma_2$ $(N = 12^4)$	0.001350410	0.001372659

Thus, we here use results from simulations when calculating σ_{ELS}. They have the same sizes N and are averaged over equally many samples as the LLS strain curves they are compared to. The difference $\sigma_{\text{ELS}} - \sigma_{\text{LLS}}$ for various bundle sizes – the same sizes and number of samples as in the previous section – in four dimensions is shown in Fig. 4.9.

The total differences $\Delta\sigma_1$ and $\Delta\sigma_2$ for these results are shown in Fig. 4.10. Now they are nearly identical, showing no real difference between the two ways of measuring the total difference. It is also impossible to discern how the difference depends on bundle size from these results. In fact, all of the five sizes we have studied here have $\Delta\sigma$-values within 6% of one another, with $N = 4^4$ differing most from the other four sizes, which are within 2% of each other.

Interestingly, the $\Delta\sigma$-values for the two largest bundles, $N = 10^4$ and $N = 12^4$, are very similar to $\Delta\sigma_1$ when using the analytical ELS strain curve, differing by less than 1%. All of these data points are shown in Table 4.1.

4.3 Dimensional dependence of strain curves

To carry out an analysis like the one in Section 4.2 for every threshold distribution and dimension we investigate is outside the scope of this project. Hence, we will here focus on a single size in each dimension, using bundles of sizes as close to $N = 10^4$ as possible. The results from the previous section suggests this should be large enough that finite size effects are fairly small, so we use the analytical, large-N results for the ELS strain

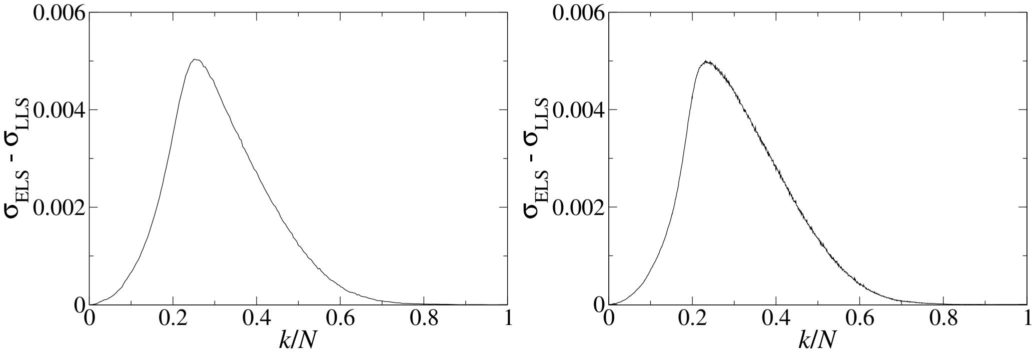

(a) $N = 4^4$ (b) $N = 6^4$

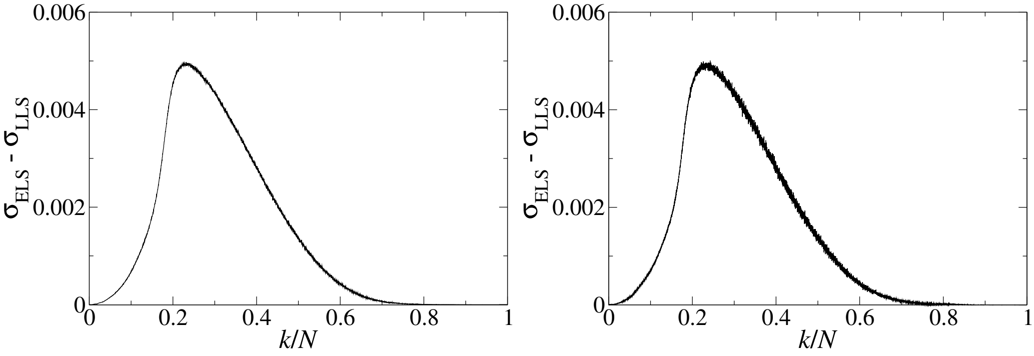

(c) $N = 8^4$ (d) $N = 10^4$

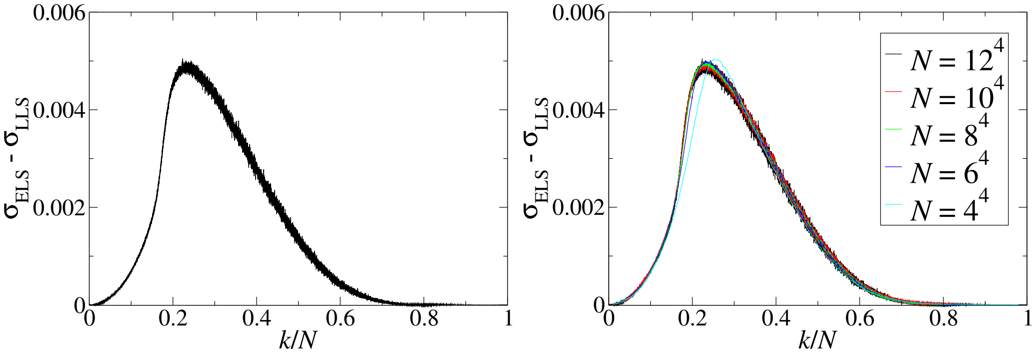

(e) $N = 12^4$ (f) A comparison.

Figure 4.9: The difference between strain curves for LLS and ELS from simulations, $\sigma_{\text{ELS}} - \sigma_{\text{LLS}}$, in four dimensions with $P(x) = x$. Subfigures (a)-(e) show different bundle sizes while Subfigure (f) shows a comparison of (a)-(e).

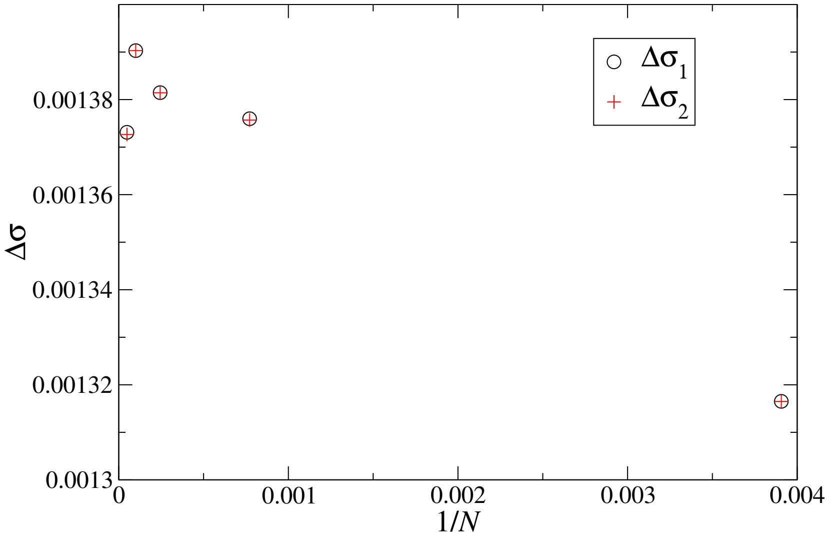

Figure 4.10: $\Delta\sigma_1$ and $\Delta\sigma_2$ for $P(x) = x$ in four dimensions as functions of $1/N$ when using averaged ELS strain curves from simulations.

curves, Eqs. (2.7) and (2.8), as σ_{ELS}. A few different threshold distributions $P(x)$ are investigated.

Some of the results presented in this section have been used in an article that has been submitted to PRL, which is found in its entirety in Appendix A.

4.3.1 Uniform distribution

We let $P(x) = x$, the uniform distribution on the unit interval[1]. The ELS strain curve, for which Eq. (2.7) is used, is presented together with the LLS strain curves for one through five dimensions in Fig. 4.11. The LLS results are for bundle sizes $N = 10^4$, 10^4, 22^3, 10^4 and 6^5 and are averaged over $3.5 \cdot 10^5$, $1.5 \cdot 10^5$, $8 \cdot 10^4$, $4 \cdot 10^4$ and $4 \cdot 10^4$ samples, respectively. The differences between ELS and these LLS strain curves are shown in Figs. 4.12 and 4.13. It is clearly visible that the difference diminishes as the dimension increases.

Fig. 4.14 displays the total differences $\Delta\sigma_1$ and $\Delta\sigma_2$. Fitting the data points to a power law, a behaviour $\Delta\sigma_i \propto D^{-\mu_i}$ with $\mu_1 \simeq 3.41$ and $\mu_2 \simeq 3.46$ is observed. Since the exponents are a little different, the data points from Fig. 4.14 are listed in Table 4.2.

As the dimension increases, the two measures for the total difference become less similar, with a significant relative difference in five dimensions. To understand this, we plot the difference in ELS and LLS strain curves for five dimensions only, shown in Fig. 4.15. The curve is negative for k/N close to one, with an amplitude that is comparable

---

[1] We also did simulations in three, four and five dimensions when $P(x)$ was uniform on the interval $(0.4, 1)$, and the results show that the total difference decreases with the dimension. However, since trying to do a regression with only three data points could easily give very wrong results – especially when the points are placed close to each other – we do not show these results in any figures or try to extrapolate how they depend on the dimension.

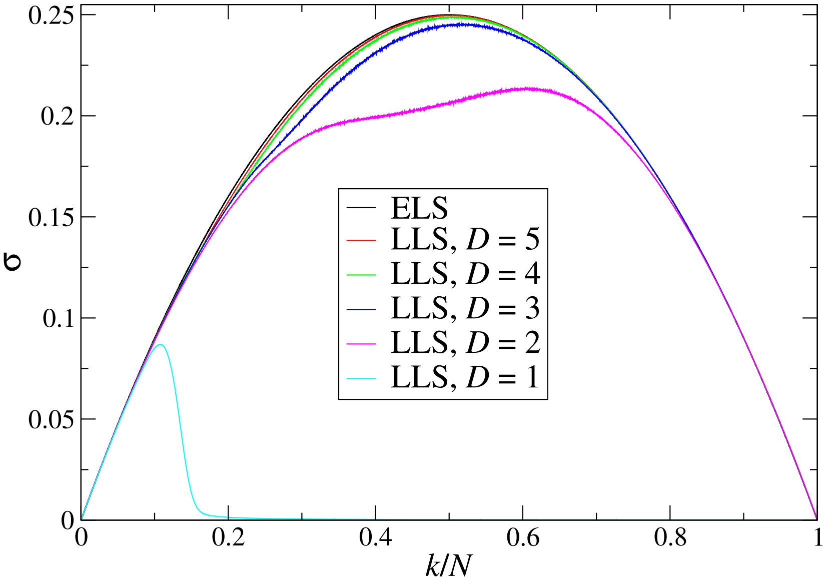

Figure 4.11: The averaged strain curves for LLS simulations when $P(x) = x$, with the analytical ELS result for comparison.

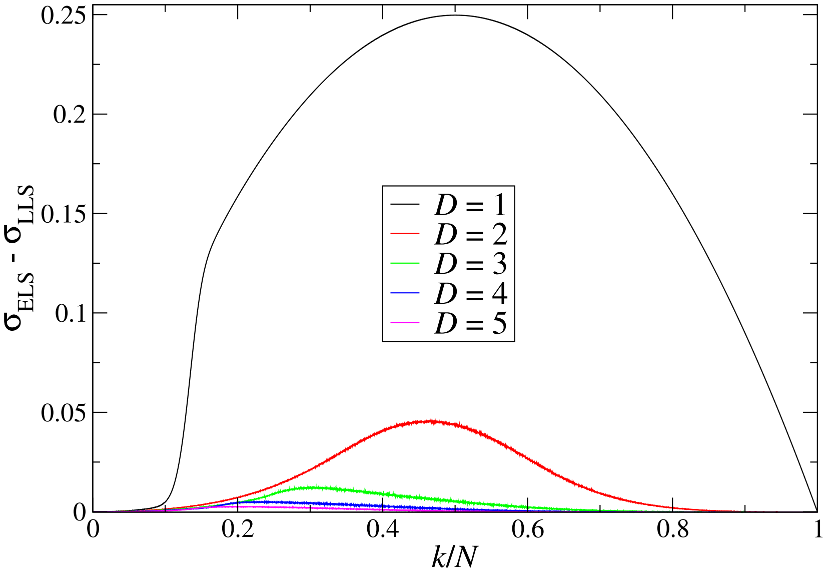

Figure 4.12: The difference $\sigma_{\mathrm{ELS}} - \sigma_{\mathrm{LLS}}$ for one through five dimensions when $P(x) = x$.

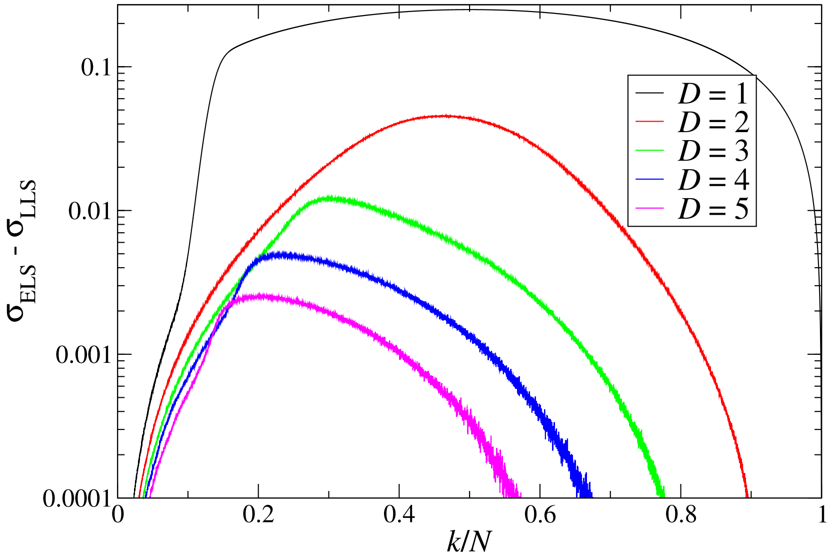

Figure 4.13: The difference $\sigma_{\mathrm{ELS}} - \sigma_{\mathrm{LLS}}$ for one through five dimensions when $P(x) = x$, with a logarithmic axis to easier see the results for the highest dimensions.

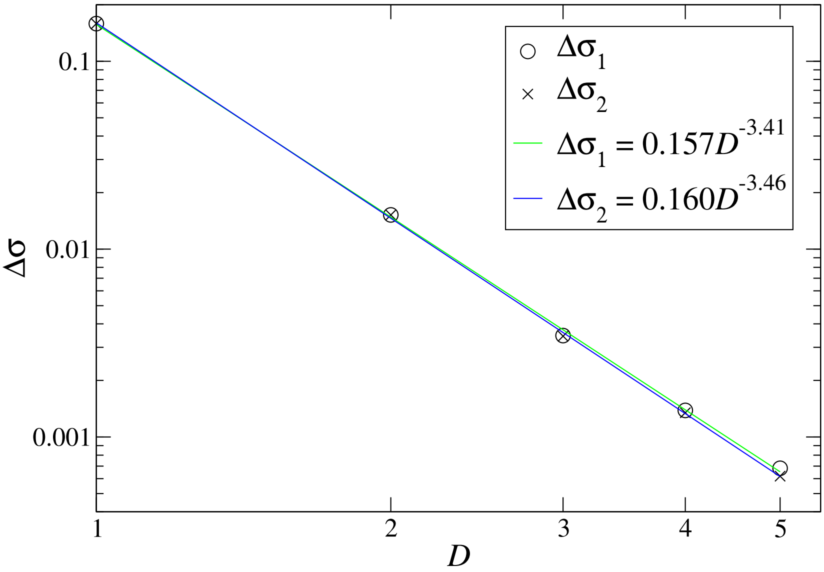

Figure 4.14: The total differences $\Delta\sigma_i$ as functions of the dimension D when $P(x) = x$. The two lines are power laws fitted to $\Delta\sigma_1$ (green) and $\Delta\sigma_2$ (blue).

Table 4.2: $\Delta\sigma_i$-values for one to five dimensions with $P(x) = x$. These data points are plotted in Fig. 4.14.

D	$\Delta\sigma_1$	$\Delta\sigma_2$
1	$1.58582107 \cdot 10^{-1}$	$1.58582084 \cdot 10^{-1}$
2	$1.52135839 \cdot 10^{-2}$	$1.52008615 \cdot 10^{-2}$
3	$3.46579151 \cdot 10^{-3}$	$3.44041546 \cdot 10^{-3}$
4	$1.38500226 \cdot 10^{-3}$	$1.34638279 \cdot 10^{-3}$
5	$6.81122003 \cdot 10^{-4}$	$6.18623163 \cdot 10^{-4}$

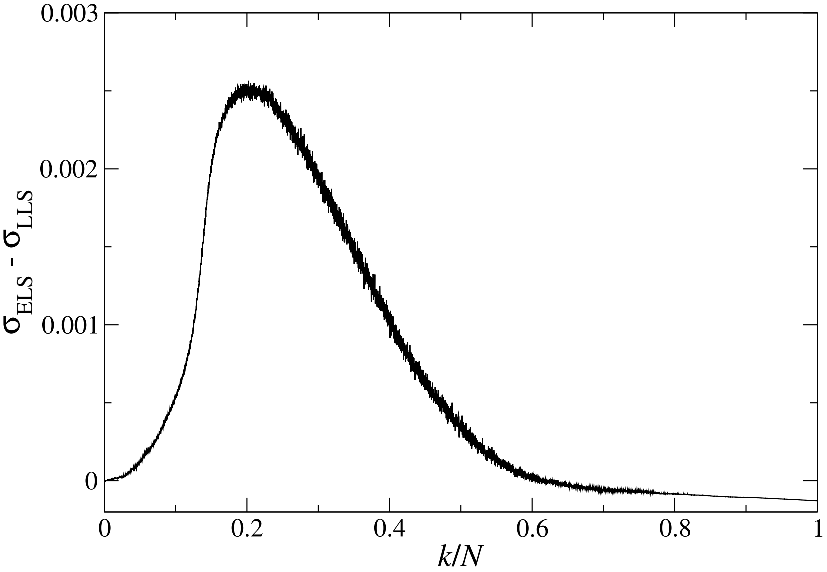

Figure 4.15: The difference $\sigma_{\mathrm{ELS}} - \sigma_{\mathrm{LLS}}$ for $D = 5$ when $P(x) = x$.

to, although still smaller than, the positive difference elsewhere.

When looking at the burst size distribution, as we will in Section 4.4, it is of interest to know how the strain curve of single samples look, as that is what defines the burst size distribution. Therefore Fig. 4.16 contains the LLS strain curves for a single sample in one through five dimensions, with the averaged ones from Fig. 4.11 for comparison, in addition to the ELS strain curve for a single sample with $N = 10^4$. From two dimensions and upwards, the number of large fluctuations in the LLS strain curve seems to decrease when the dimension increases. The single-sample ELS strain curve has much smaller fluctuations than the LLS results in any of the five dimensions.

4.3.2 Exponential distribution

We now use an exponential threshold distribution $P(x) = 1 - \exp(x_< - x)$, where $x \in [x_<, \infty)$, and study the results for two different values of the cut-off $x_<$.

Lower cut-off $\mathbf{x_< = 0}$

We let $x_< = 0$, meaning that the threshold distribution is $P(x) = 1 - \exp(-x)$. Using Eq. (2.8) with $x_< = 0$ for the ELS strain curve, we show it together with the LLS results from simulations in Fig. 4.17. For each dimension the same bundle size and number of samples as for $P(x) = x$ is used.

Just like for the uniform distribution, the difference between equal and local load sharing diminishes rapidly with increasing dimension. The difference is plotted in Figs. 4.18 and 4.19, the latter with a logarithmic axis to better see the highest dimensions.

Using $\Delta\sigma_1$ and $\Delta\sigma_2$ to measure the total difference, we plot them as functions of dimension in Fig. 4.20. The two measures are nearly identical except when $D = 5$, where there is a noticeable difference even in the logarithmic plot.

The total differences are observed to follow a power law $\Delta\sigma_i \propto D^{-\mu_i}$, with fits to the values providing $\mu_1 \simeq 3.61$ and $\mu_2 \simeq 3.73$.

Lower cut-off $\mathbf{x_< = 1}$

We now turn our attention to the case where $x_< = 1$, meaning that $P(x) = 1 - \exp(-x + 1)$. For the ELS strain curve Eq. (2.8) is once again used, but this time with $x_< = 1$. Plotting this together with the LLS results from simulations in one through five dimensions provides Fig. 4.21. The bundle sizes and number of samples are identical to the ones used for the uniform distribution on the unit interval and the exponential distribution with $x_< = 0$. Also here a quickly decaying difference between ELS and LLS when the dimension increases is observed. This difference is shown in Fig. 4.22. The total differences $\Delta\sigma_1$ and $\Delta\sigma_2$ are plotted as functions of dimension in Fig. 4.23, together with power law fits to the data points. The two measures give almost exactly the same results, and in fact it is not possible to see any difference between the two fits from the figure; they seem to be exactly on top of each other. They give the connection $\Delta\sigma_i \propto D^{-\mu_i}$ with $\mu_1 \simeq 2.33$ and $\mu_2 \simeq 2.34$, but we observe that these power laws do not fit very well with the results for two dimensions and, to a lesser degree, one dimension.

Fig. 4.21 also provides some information about the stability of the fibre bundles. The ELS result, as seen from Eq. (2.8), is both globally unstable and locally unstable everywhere; the force required to break the next fibre decreases for every fibre that breaks.

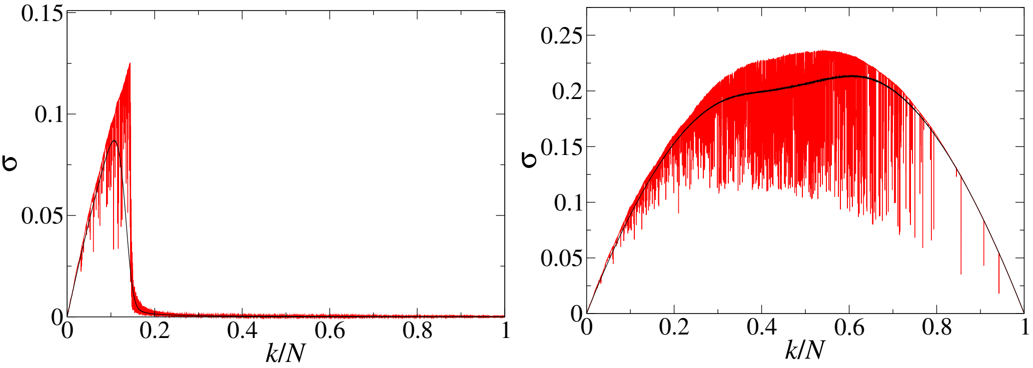

(a) $D = 1$

(b) $D = 2$

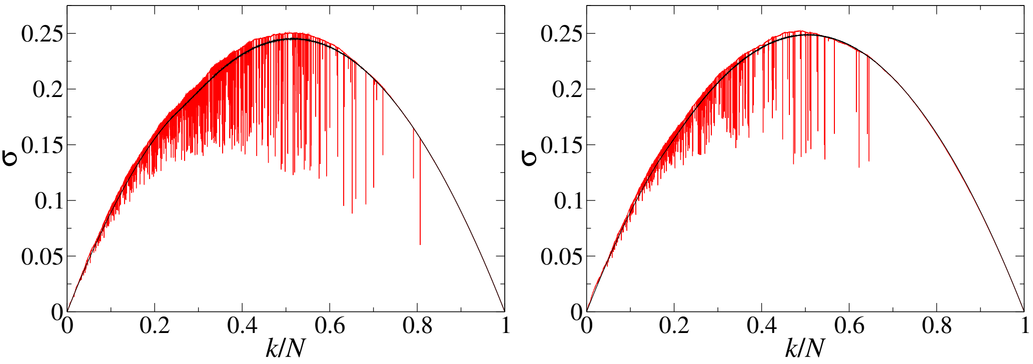

(c) $D = 3$

(d) $D = 4$

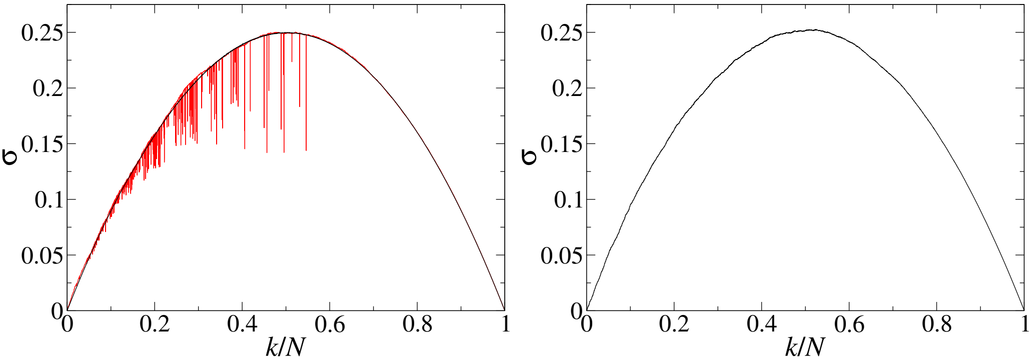

(e) $D = 5$

(f) ELS

Figure 4.16: (a)-(e) show LLS strain curves for single samples (red) and averaged (black) for one to five dimensions, while (f) shows an ELS strain curve from a single sample. $P(x) = x$ in all the subfigures.

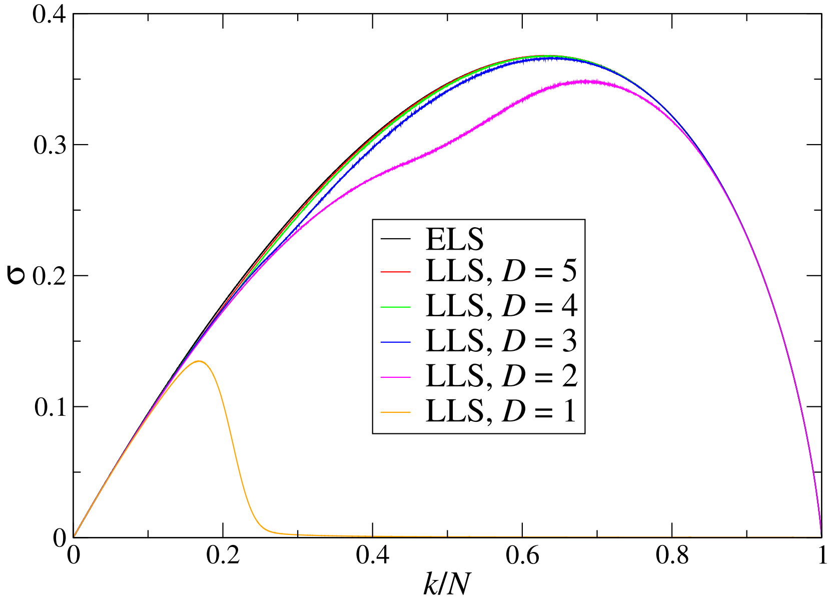

Figure 4.17: The averaged strain curves for LLS simulations in one through five dimensions when $P(x) = 1 - \exp(-x)$, with the analytical ELS result for comparison.

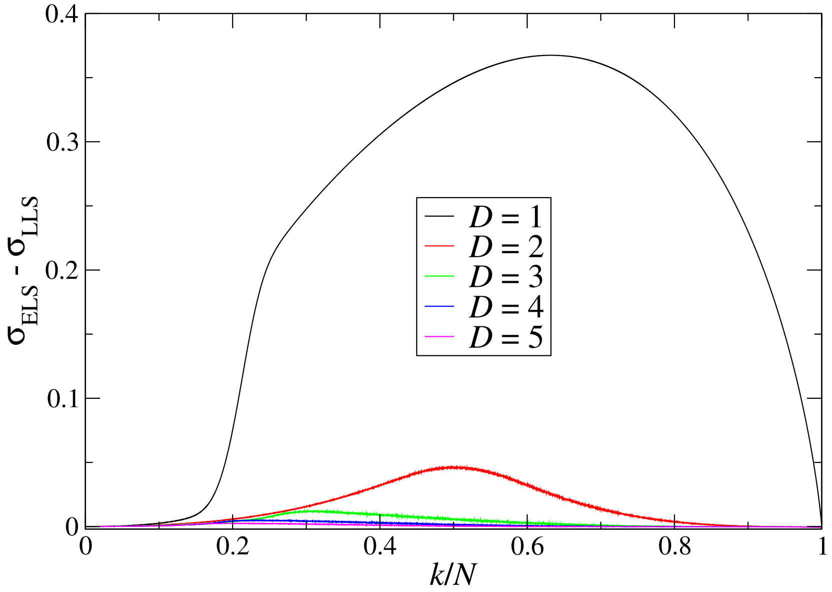

Figure 4.18: The difference $\sigma_{\mathrm{ELS}} - \sigma_{\mathrm{LLS}}$ in one to five dimensions when $P(x) = 1 - \exp(-x)$.

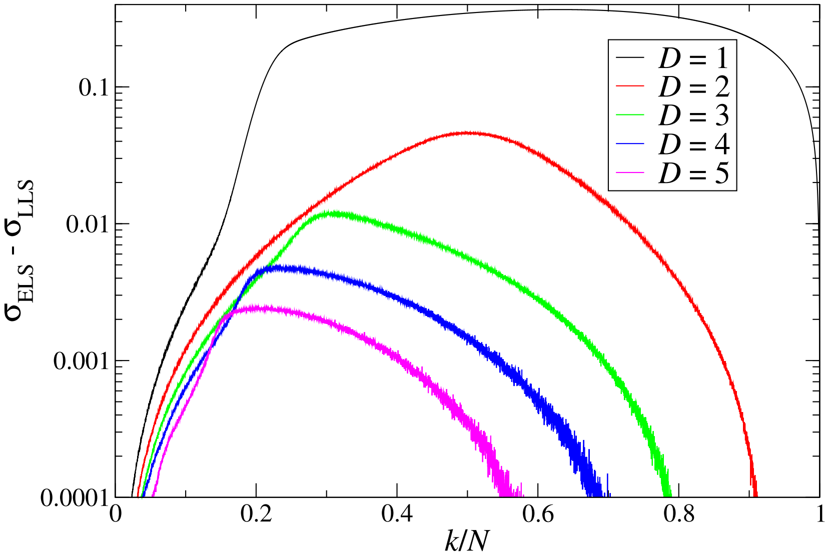

Figure 4.19: The difference $\sigma_{\mathrm{ELS}} - \sigma_{\mathrm{LLS}}$ in one to five dimensions when $P(x) = 1 - \exp(-x)$ with a logarithmic axis to easier see the results for the highest dimensions.

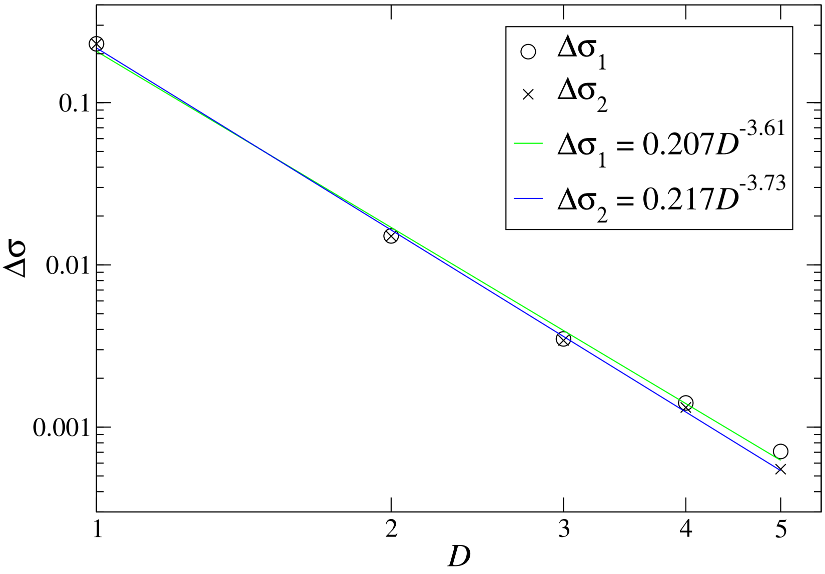

Figure 4.20: The total differences $\Delta\sigma_i$ as functions of the dimension D when $P(x) = 1 - \exp(-x)$. The two lines are power laws fitted to $\Delta\sigma_1$ (green) and $\Delta\sigma_2$ (blue).

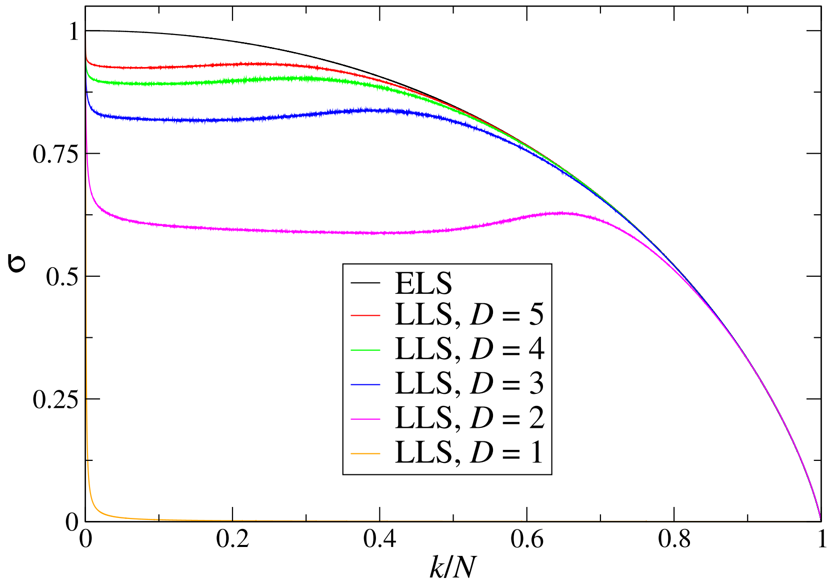

Figure 4.21: The averaged strain curves for LLS simulations in one through five dimensions when $P(x) = 1 - \exp(-x + 1)$, with the analytical ELS result for comparison.

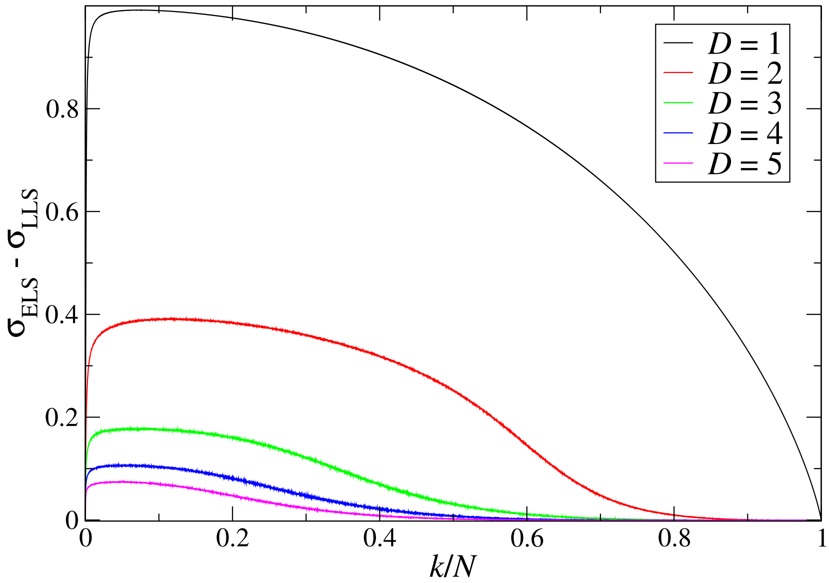

Figure 4.22: The difference $\sigma_{\mathrm{ELS}} - \sigma_{\mathrm{LLS}}$ for one to five dimensions when $P(x) = 1 - \exp(-x + 1)$.

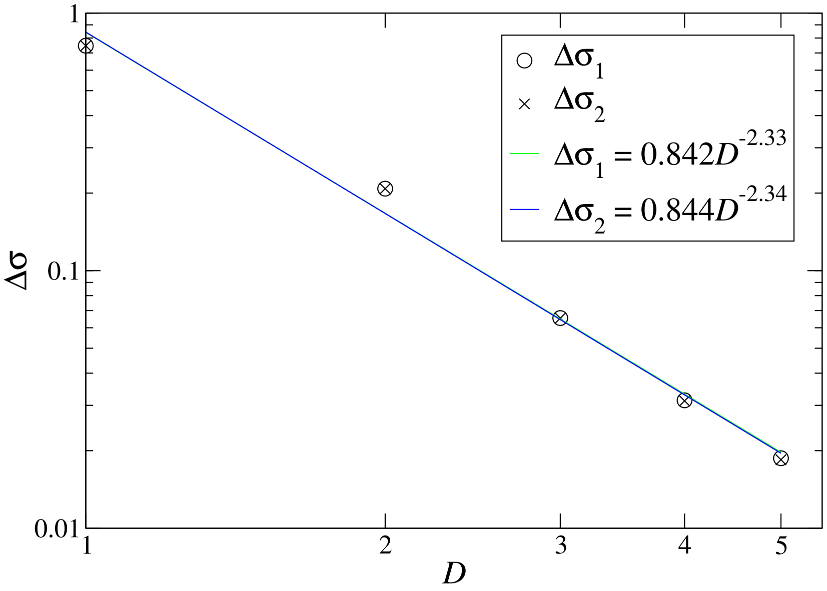

Figure 4.23: The total differences $\Delta\sigma_i$ as functions of the dimension D when $P(x) = 1 - \exp(-x+1)$. The two lines are power laws fitted to $\Delta\sigma_1$ (green) and $\Delta\sigma_2$ (blue), although they are so similar that only one can be seen.

The LLS results are also globally unstable for all five dimensions – the force required to break the first fibre is the highest point of the strain curve – but only in one dimension is a local instability seen everywhere. From two dimensions and upwards there is exists a region where σ increases with k/N. It moves when the dimension changes and is most pronounced in two dimensions.

4.4 Burst size distribution in higher dimensions

In this section the burst size distribution for local load sharing changes with dimension when the threshold distribution is $P(x) = x$ is investigated. Fig. 4.24 shows this distribution for two ($N = 10^4$), three ($N = 22^3$), four ($N = 10^4$) and five ($N = 6^5$) dimensions calculated from $1.5 \cdot 10^5$, $8 \cdot 10^4$, $4 \cdot 10^4$ and $4 \cdot 10^4$ samples, respectively.

Surprisingly, they all look very similar and are notably different from the corresponding one-dimensional result, which is shown in Fig. 4.6. In particular, there is a power law-like behaviour for much larger bursts than in one dimension, where it very quickly begins to veer of from the power law. Like in one dimension, we try to find the exponent of the power law dependence $D(\Delta) \propto \Delta^{\xi}$ observed for small Δ. Fig. 4.25 shows the burst size distribution for two to five dimensions for $\Delta \leq 8$ and their corresponding power law fits. All of the dimensions give an exponent of $\xi \approx 2.6$, which is very different from the one-dimensional result of $\xi \approx 4.6$, but somewhat close to the ELS exponent of $\xi \approx 2.7$ for very small bursts.

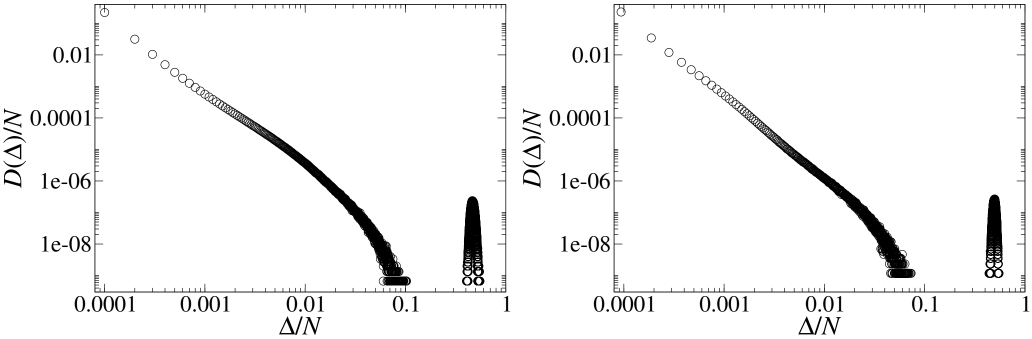

(a) $D = 2$ (b) $D = 3$

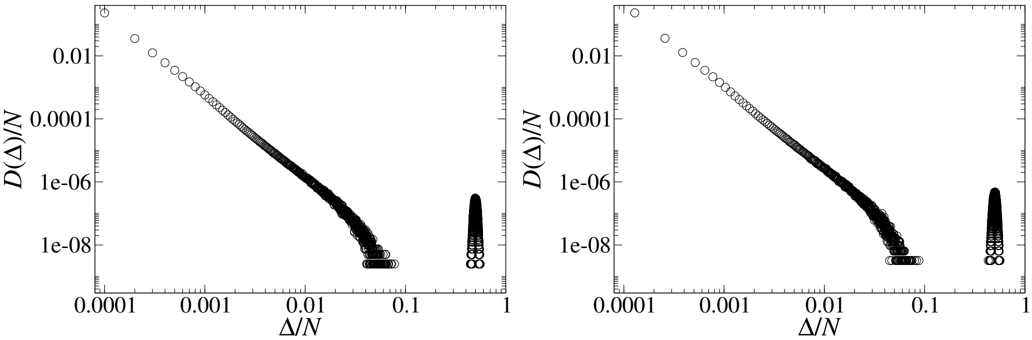

(c) $D = 4$ (d) $D = 5$

Figure 4.24: LLS Burst size distribution for two to five dimensions when $P(x) = x$.

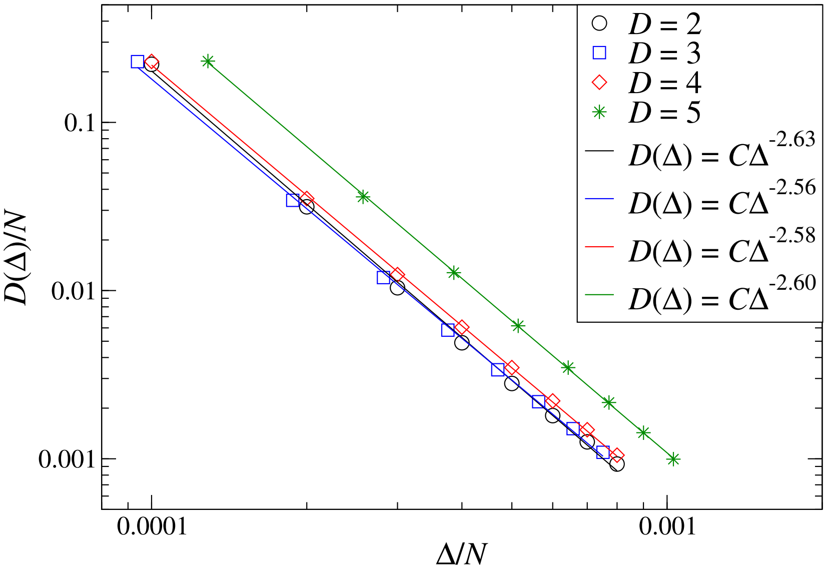

Figure 4.25: LLS burst size distribution for $\Delta \leq 8$ when $P(x) = x$ and corresponding power law fits for two dimensions (black), three dimensions (blue), four dimensions (red) and five dimensions (green).

5 Discussion

We will here discuss and interpret the results from Chapter 4, mostly discussing the results in the order they were presented. First the one-dimensional results, both for strain curves and burst size distributions, are compared to results in existing literature in Section 5.1. Then the size dependence analysis in four dimensions with a uniform distribution is discussed in Section 5.2, before we continue with the dimensional dependence of strain curves in Section 5.3, the LLS burst size distribution in higher dimensions for $P(x) = x$ in Section 5.4, and finish with a short mention of sources of errors and inaccuracies in Section 5.5.

5.1 One-dimensional results

Section 4.1 shows results from simulations in one dimension, which we will now consider.

5.1.1 Strain curves

For equal load sharing we compared numerical results to the analytical formulae derived in the limit of large bundles. The differences between these two are seen to be small when $P(x) = x$, and we observe that the difference is overall much smaller for $N = 10^5$ than for $N = 10^4$, in particular when k/N is close to one, as it seems to go to $1/N$ there. That we get a better agreement for the larger bundle is expected since analytical results are valid in the limit $N \to \infty$.

When using the exponential distributions $P(x) = 1 - \exp(-x + x_<)$, the differences between simulations and analytical expressions are also fairly small, with the largest difference as $k/N \to 1$, just like for the uniform distribution with the same bundle size, $N = 10^4$. Interestingly, the difference seems to go to $1/N$ for small k with $x_< = 1$, compared to zero for the two other threshold distributions we have studied, but with no other sizes to compare to we have no way of determining whether this is a coincidence or not.

For local load sharing, we do not see any difference between the curves shown in Fig. 4.3 and the ones found in Ref. [13]. Hence, the one-dimensional LLS simulations seem to give correct strain curves.

5.1.2 ELS burst size distribution

When using equal load sharing, the burst size distribution should follow a power law as in Eq. (2.9) with $\xi = 2.5$ for large N and Δ. Our observed exponents of $\xi = 2.54$ ($N = 10^4$) and $\xi = 2.49$ ($N = 10^5$) for bursts of sizes $50 \leq \Delta \leq 200$ are very reasonable in this light, giving values close to the analytical result while also showing that $\xi = 2.5$ is the result acquired in the limit $N \to \infty$, as the exponent is closer to the analytical result for the largest fibre bundle.

For very small bursts ($\Delta \leq 8$) there is a power law dependence with a different exponent, $\xi \approx 2.7$. It is reasonable that the burst size distribution does not give the same exponent here, since the Stirling approximation for $\Delta!$ used when deriving the analytical result [11] is only good for sufficiently large Δ. Hence the slightly larger value is an acceptable result when compared to the theory.

We expect the fatal bursts that break the rest of the bundle to be of size $\Delta/N \approx 1 - k_{\max}/N$, where $k_{\max}$ is the k-value for which the averaged strain curve has its maximum. Fatal bursts begin when a single sample reaches the highest point on its strain curve, and these should be distributed close to the maximum of the averaged strain curve for most threshold distributions.

The spike in the burst size distribution representing fatal bursts is situated at $\Delta \simeq N/2$, which is what one would expect since the ELS strain curve for a uniform distribution, Eq. (2.7), has its maximum at $k/N = 0.5$. While the power law exponent has been shown to be universal for most threshold distributions, we expect this spike to occur at different points for distributions with their strain curve maxima at different values of k/N. However, since we have only calculated the burst size distributions for $P(x) = x$, we cannot confirm that this is the case.

5.1.3 LLS burst size distribution

For local load sharing we studied the burst size distribution when $P(x) = x$ and observe the same qualitative effects as Kloster et al. [17] show analytically; for small Δ there is a power law dependence as in Eq. (2.12) where $\xi \approx 4.6$ ($N = 10^4$), but the burst size distribution quickly begins to veer off from this power law to diminish even faster.

The value $\xi \approx 4.6$ seems reasonable when compared to previously found results: $\xi \simeq 4.5$ for $N = 5000$ [19] and $\xi = 5$ for $N = 20000$ [17]. Since the exponent ξ has been observed to increase with N for $P(x) = x$ [18] we expect it to be somewhere in the interval $(4.5, 5)$ for $N = 10^4$, which is precisely what we have found.

The fatal bursts are observed to be distributed around $\Delta \simeq 0.88N$, which is in fairly good correspondence with the maximum of the averaged strain curve, see Fig. 4.11, at $k/N \simeq 0.11$. This is not a perfect match, which indicates that the maximum of the strain curves for single samples is distributed around a k/N-value slightly higher than where the maximum of the averaged curve is found.

This would mean that single samples like the one shown in Fig. 4.16a, which has its maximum at a higher k than the corresponding average, is not as uncommon as one might first guess. While we cannot decisively conclude that this is the case without examining the distribution of strain curve maxima positions in detail, we see an indication that this might be correct.

5.1.4 Overall remarks

We see that both the strain curves and burst size distributions for equal and local load sharing in one dimension give reasonable and expected results when compared to previous analytical and computational work, and can hence conclude that our numerical implementation works as expected.

5.2 Size dependence in four dimensions

We have proposed two quantities, $\Delta\sigma_1$ and $\Delta\sigma_2$, to measure the total difference between ELS and LLS strain curves, and have studied them for both analytical, large-N ELS results and ELS results from simulations – and thus of finite size – in four dimensions when $P(x) = x$.

5.2.1 Analytical ELS

With analytical ELS results we see that $\Delta\sigma_2$, or, equivalently for large bundles, the area under the difference curve, is a misleading quantity for the total difference for very small bundles. When $N = 4^4 = 256$ it is nearly zero, which is not representative of the corresponding curve from which $\Delta\sigma_2$ is calculated at all.

For larger bundles, however, it is very similar to $\Delta\sigma_1$, with both of them seemingly converging to roughly the same value as the bundle size goes to infinity, meaning that it should not matter which measure is used in this limit. Since the two measures behave very differently for small enough sizes – $\Delta\sigma_1$ decreases with larger bundles while $\Delta\sigma_2$ increases – we can interpret the difference between these two values as a measure of how much finite size effects affect the results. Based on the behaviour as N changes that we have seen here, the values attained when $N \to \infty$ are expected to be somewhere between $\Delta\sigma_1$ and $\Delta\sigma_2$ found for a finite size.

When the bundle size is sufficiently large, i.e. of order 10^4, the two measures are located within a few percent of each other, and they are also only a few percent off from the estimate of $\Delta\sigma_1$ as $N \to \infty$ provided by the linear fit in Fig. 4.8a. Hence we can say that using bundles of size $N \approx 10^4$ should be sufficient to estimate what happens in the limit of large bundles, at least for this dimension and threshold distribution.

5.2.2 Numerical ELS

When using ELS strain curves from actual simulations, and thus of finite size, there is no discernible difference between $\Delta\sigma_1$ and $\Delta\sigma_2$ for the sizes we have investigated. It is very interesting that all the bundle sizes give similar results, as seen from Figs. 4.9f and 4.10. As one would expect, since the numerical ELS results should grow closer to the analytical result as the bundle size increases, the two measures are similar to their counterparts using analytical ELS strain curves for the larger bundles. That similar values are also attained for much smaller bundles is somewhat surprising. It would mean that effects due to finite size affect equal and local load sharing in nearly the exact same way, and that the behaviour of the difference $\sigma_{\text{ELS}} - \sigma_{\text{LLS}}$ at infinite size should also be valid for fairly small finite bundle sizes when numerical and finite-sized results are used for both the equal and local load sharing model.

5.2.3 Validity

The results regarding size dependency discussed here are only shown to be valid in four dimensions and for the uniform threshold distribution $P(x) = x$, so we cannot guarantee that they are still valid for other dimensions or threshold distributions.

5.3 Dimensional dependence of strain curves

We have investigated how the strain curves vary with dimension for a few different threshold distributions. They are discussed separately in the following sections.

5.3.1 Uniform distribution

When $P(x) = x$, we observe a power law behaviour for $\Delta\sigma_i$ as a function of dimension with slightly different exponents for $\Delta\sigma_1$ and $\Delta\sigma_2$ because of somewhat different values for the five-dimensional case. This is due to two different effects.

Smaller bundle: The size of the five-dimensional fibre bundle used is $6^5 = 7776$, which is somewhat smaller than the other dimensions, which use $N \simeq 10^4$. As seen in four dimensions, a smaller bundle means larger effects due to finite size and thus a larger difference between $\Delta\sigma_1$ and $\Delta\sigma_2$.

Higher dimension: When the dimension increases, the difference between equal and local load sharing diminishes, and so a finite size effect of a given order will affect the result more than in a lower dimension, because the true difference does not dominate the finite size effects as effectively. We can see this in Fig. 4.15 and Table 4.2, where the effects due to finite size – the negative part of the curve for sufficiently large k/N – are comparable to the rest of the difference, causing $\Delta\sigma_1$ and $\Delta\sigma_2$ to differ significantly.

The difference, however, is only a matter of how precisely one wants to determine the exponent of the power law. To get a more accurate value, a larger bundle size would be needed in five dimensions. Considering the size dependency analysis, which leads us to expect that the true exponent is somewhere in between the estimates given by $\Delta\sigma_1$ and $\Delta\sigma_2$ here, we expect to find a power law dependence $\Delta\sigma_2 \propto D^{-\mu}$ with $\mu \approx 3.4$ in the limit of large bundles, meaning that the critical dimension where ELS and LLS become equal is not finite at all, but infinity.

It is difficult to estimate the uncertainty of this exponent, but given the result found in Appendix A (which partially uses the same data as us), $\mu \approx 3.5$, and that the power law is observed only over half a decade, the uncertainty is probably at least 0.1. We therefore guess that $\mu = 3.4 \pm 0.2$. Since the power law is observed over half a decade, we cannot say that it is very robust, but extending the region, i.e. the number of dimensions, further would require computational resources far beyond what has been made available for this thesis.

It is a little surprising that the one-dimensional LLS model fits into this power law, since the LLS model in one dimension is qualitatively different from all higher dimensions in the sense that the number of neighbours to a hole cannot increase with the hole size. As we will discuss later, the burst size distribution seems to behave qualitatively different in one dimension when compared to higher dimensions.

Fig. 4.13 provides valuable insight into why the equal and local load sharing models become more and more similar as the dimension increases. For small k/N and LLS, fibres mainly fail because of their small thresholds, not because of force redistribution from failed neighbours, and hence ELS and LLS behave very similarly in this region.

We also see that the point – in terms of k/N – where the two models become nearly identical again decreases with increasing dimension. This is ostensibly because the point where all holes have merged into a single, large hole that has almost all intact fibres in its perimeter decreases when the number of neighbours per fibre goes up. When this point is reached, the LLS force distribution is essentially ELS and the two models converge. That the point of this transition decreases is analogous to how the percolation thresholds for hypercubic lattices decrease with increasing dimension [23] in the percolation model. If this is the reason why equal and local load sharing become more similar as the dimension increases, it is expected that the result $\Delta\sigma_2 \to 0$ as $D \to \infty$ is valid for any threshold distribution $P(x)$.

Single samples
Looking at the single samples displayed in Fig. 4.16, it seems as though the number of large fluctuations decrease as the dimension increases. We should be careful about including the five-dimensional result in this argument, as the total number of fibres is a little lower than in the other dimensions, but the same effect can be seen from the samples from two to four dimensions, where the bundle sizes are nearly identical. From only a single sample in each dimension, though, we cannot conclude with a decrease, but the results are indications that such a trend might exist.

This decrease is reasonable, however, as the perimeter size of a hole increases with the dimension, making thresholds of single fibres in a given configuration less important. (In the sense that it is less probable to have a combination of fibre thresholds that make the required force to break the next fibre deviate significantly from the average.) With ELS the single samples rarely deviate much from the average, at least for large bundles where many fibre thresholds must be drawn from $P(x)$, and it we expect single samples with LLS in higher dimensions to behave more like this than in lower dimensions.

This is of importance for the LLS burst size distribution, which should then behave more like the ELS burst size distribution in higher dimensions, although how similar they become and how quickly we cannot judge from this simple argument.

5.3.2 Exponential distribution with $\mathbf{x}_< = \mathbf{0}$

When $P(x) = 1 - \exp(-x)$ we observe a power law behaviour for $\Delta\sigma_i$ as a function of dimension with somewhat different exponents for $\Delta\sigma_1$ and $\Delta\sigma_2$ due to differing values in five and, to a lesser degree, four dimensions. While we have not done a size dependency analysis for this probability distribution, like for $P(x) = x$ in Section 4.2, these differences are likely effects due to finite size, and we therefore expect the exponent attained in the limit $N \to \infty$ to be somewhere in between the ones we have found for $\Delta\sigma_1$ and $\Delta\sigma_2$. Hence, we conclude that in the limit of large bundles there likely is a power law dependence $\Delta\sigma_2 \propto D^{-\mu}$ with $\mu \approx 3.7$, and the critical dimension where ELS and LLS become equal is infinity.

Also for this threshold distribution the uncertainty of the exponent is difficult to gauge, but again considering the results from Appendix A, $\mu \approx 3.5$, and that we have only observed the power law behaviour over half a decade, the uncertainty is likely at least 0.2. Thus we guess that $\mu = 3.7 \pm 0.3$.

The reason for this convergence seems to be the same as for $P(x) = x$, according to Fig. 4.19; the point in k/N where the two models become essentially equal decreases with the dimension, making the total difference smaller.

5.3.3 Exponential distribution with $\mathbf{x}_< = \mathbf{1}$

For $P(x) = 1 - \exp(-x + 1)$ there are non-negligible effects due to finite size [8], so it is not possible to conclude with how the total difference between ELS and LLS behaves without doing a size scaling analysis for each dimension. This might be related to the results observed in one dimension, where the difference between analytical and numerical ELS seems to go to $1/N$ as $k/N \to 0$. We do, however, see that the difference decreases with increasing dimension, and the exponent of the power law fit is profoundly different from the ones found for the two distributions $P(x) = x$ and $P(x) = 1 - \exp(-x+1)$. This might be an indication that μ is not universal, but changes depending on the threshold distribution.

A very surprising result when using this threshold distribution is the regions of local stability that occur for LLS in two to five dimensions, as seen in Fig. 4.17. While the ELS model is still more stable in the sense that σ is higher than in LLS at any point in the breaking process, it is strange that the LLS model has a local stability that is not present in the ELS model. Moreover, this stability seems to decrease as the dimension increases beyond two, becoming less pronounced. We do not have an explanation for this behaviour, but it likely has something to do with how the hole structure in LLS changes with the dimension for this threshold distribution.

5.4 Burst size distribution in higher dimensions

The burst size distributions in two to five dimensions when $P(x) = x$ shown in Figs. 4.24 and 4.25 are surprising; they are all very similar and the power law dependence for small bursts, $\Delta \leq 8$, give nearly identical exponents of $\xi \approx 2.6$. From the discussion on single samples we might expect the distribution to gradually behave more like in the ELS model, but this seems not to be the case in our results. From two dimensions onward, it behaves fundamentally different from in one dimension, where we have seen that the exponent is much larger. Interestingly, the values seen here for two to five dimensions are in between (and quite close to) the small-burst exponent seen for ELS, $\xi \simeq 2.7$, and the analytical, large-N, large-Δ result $\xi = 2.5$. The burst size distribution also keeps a power law-like behaviour for much larger bursts in higher dimensions, while in one dimension it quickly veers off from this behaviour once $\Delta > 10$.

Since ξ depends heavily on N in one dimension with local load sharing, it seems reasonable to assume that there is also a noticeable size dependence for higher dimensions. If the exponents then increase with the bundle size as in one dimension, it is possible that they go to some upper limits as $N \to \infty$ – one for each dimension – and that these limits gradually move closer to the ELS value $\xi \simeq 2.7$ for small bursts. It might also be that for sufficiently large bundles the *entire* LLS burst size distribution grows closer to the ELS burst size distribution as the dimension increases, which would be in accordance with the previous argument regarding how single samples change with dimension. Since we do not have any data for other bundle sizes we cannot say whether this is the case or not, but it might be an interesting subject for someone to investigate later.

5.5 Errors and inaccuracies

There are mainly two sources of errors in the results presented in this thesis: finite bundle size N and the number of samples used. Effects due to finite size grow continually smaller as the bundle size increases, so larger values of N would give more accurate data. Similarly, increasing the number of samples used when calculating averages and burst size distributions should also give more accurate results.

We can see a few examples of the latter affecting the results in the burst size distributions; very rare bursts, which typically are quite large, are entirely absent even though they should occur with a non-zero probability. This is because in all the samples used, bursts of many sizes were never observed at all since they are too rare. The rarest bursts that are actually observed will give uncertain results – which is clearly seen in for instance Fig. 4.4 – as a single sighting of such a rare burst can change the value of the burst size distribution significantly.

6 Conclusion

The purpose of this thesis was to investigate whether there exists a finite critical dimension where the equal and local load sharing fibre bundle models behave identically. For this purpose we introduced a generalization of the local load sharing model to arbitrarily high dimensions by placing the fibres in a hypercubic pattern and defining a history-independent force distribution mechanism that is consistent with how the model has previously been treated in one dimension.

The simulations carried out with this model in one to five dimensions indicate that the critical dimension is not finite, but rather *infinity*. The area under the difference curves $\sigma_{\text{ELS}} - \sigma_{\text{LLS}}$, $\Delta\sigma_2$, behaves as a power law with respect to the dimension D,

$$\Delta\sigma_2 \propto D^{-\mu}, \tag{6.1}$$

in the limit $N \to \infty$. (For σ_{ELS} we have used the analytical results valid in the limit of large N.) The exponent is estimated to be $\mu = 3.4 \pm 0.2$ for the uniform threshold distribution $P(x) = x$ and $\mu = 3.7 \pm 0.3$ for $P(x) = 1 - \exp(-x)$, and hence we cannot conclude that they are different. However, the results for $P(x) = 1 - \exp(-x+1)$ indicate that μ is likely not universal, but depends on the threshold distribution in question. Since we have used $D \leq 5$, this power law dependence has only been observed over half a decade.

Seemingly, the two models converge because the number of nearest neighbours for each fibre increases with the dimension. At some point in the LLS model, the broken fibres constitute a single large hole with most of the intact fibres in its perimeter, thus distributing the forces almost identically to the ELS model. In one dimension this first happens when there are only a few intact fibres left, but as the dimension increases this point decreases because of the increased connectivity between the fibres.

If this is indeed the reason why $\Delta\sigma_2$ decreases with increasing dimension, one would expect that it should go to zero as $D \to \infty$ for any threshold distribution $P(x)$. We see indications that this might be the case for $P(x) = 1 - \exp(-x+1)$ as well, but the presence of non-negligible finite size effects requires a size scaling analysis to confirm this.

From the size dependency analysis done in four dimensions with $P(x) = x$ using numerical ELS results, it seems that the total difference between equal and local load sharing varies very little with size when using numerical results for both models. This means that there likely is a power law dependence also for fairly small fibre bundles, not only in the limit $N \to \infty$, at least for the uniform threshold distribution.

An article has been written using some of the data sets shown in this thesis, and it has been submitted to PRL. It is shown in its entirety in Appendix A.

We have also studied the burst size distribution for the uniform threshold distribution $P(x) = x$ with local load sharing, seeing a power law dependence

$$D(\Delta) \propto \Delta^{-\xi} \tag{6.2}$$

for small bursts Δ. In one dimension we get $\xi \approx 4.6$ when $N = 10^4$, which fits well with the fact that ξ increases with the bundle size [18] and the previously found values $\xi \simeq 4.5$ for $N = 5000$ [19] and $\xi = 5$ for $N = 20\,000$ [17].

When going to two dimensions, we see a qualitative shift where $\xi \approx 2.6$ when $N = 10^4$, which is also the value found in three, four and five dimensions when the bundle sizes are $N = 22^3$, 10^4 and 6^5, respectively. The higher dimensions behave very differently from one dimension, retaining a power law-like behaviour for much larger bursts, and, surprisingly, the burst size distribution seems to vary little between them, especially so for the smallest bursts.

While the exponent 2.6 is much closer to the exact ELS result $\xi = 2.5$, valid in the limits of large N and Δ, and the numerical ELS result of $\xi \approx 2.7$ that we have found for small Δ, the size dependency of the one-dimensional LLS burst size distribution renders it probable that there are similar size dependencies for higher dimensions as well. For this reason we cannot conclude about whether the LLS results converge towards the ELS burst size distribution or not, but only that there seems to be a qualitative difference between one and all higher dimensions when $P(x) = x$.

6.1 Suggestions for future work

The results presented in this thesis raise several new questions that may be suitable subjects for future research.

- Is the critical dimension also infinite when using models that lie between the equal and local load sharing models?

Since the ELS and LLS models, which are opposite extremes in terms of force distributions, seem to converge as the dimension increases, the same should hold true when comparing ELS to any model with a force distribution in between these two extremes. Checking whether this is indeed true would either support or undermine the results presented here, depending on the outcome, and is a natural continuation of the work done in this thesis.

- How does the lattice used for fibre placement and determination of nearest neighbours affect the results?

Based on the explanation we have offered for the increased similarity between ELS and LLS in higher dimensions, it is reasonable to ask whether it is simply a matter of connectivity between the fibres that determines how differently the two models behave. Would using a two-dimensional equilateral triangular lattice – where each fibre has six nearest neighbours, just like in the cubic lattice – give results like our LLS model in three dimensions? Does only the number of nearest neighbours matter or does the structure of neighbour relations affect the results as well? These are questions we will not attempt to answer here, but we consider them interesting and possibly suitable for further research.

- What is the source of the local stability observed for two and higher dimensions in the LLS model when $P(x) = 1 - \exp(-x + 1)$?

We have not provided any explanation of the very surprising local stability that occurs in the LLS model once we go from one to two dimensions with $P(x) = 1 - \exp(-x + 1)$. The mechanism behind this behaviour is something we consider to be an interesting subject for future research.

- How does the LLS burst size distribution vary with the bundle size in two and higher dimensions?

- Is the qualitative shift from one to two dimensions when $P(x) = x$ also present for other threshold distributions?
- Why is there such a large qualitative shift from one dimension to higher dimensions?

The results we have shown for the LLS burst size distribution give us more new questions than answers. We have not investigated how it varies with N, how it looks for other threshold distributions, or given an explanation for the sudden shift from one to two dimensions. Investigating these things might provide valuable, new insight into the LLS burst size distribution.

References

[1] H. J. Herrmann and S. Roux. *Statistical models for the fracture of disordered media*. Elsevier, 2014.

[2] S. J. V. Frankland, V. M. Harik, G. M. Odegard, D. W. Brenner, and T. S. Gates. The stress–strain behavior of polymer–nanotube composites from molecular dynamics simulation. *Composites Science and Technology*, 63(11):1655–1661, 2003.

[3] G. Linga. The breaking process of an idealized polymeric bundle under applied tensile stress. Master's thesis.

[4] S. M. Toffoli and R. L. Lehman. Determination of individual fiber failure in fiber bundles. *Journal of the American Ceramic Society*, 84(1):123–128, Feb 2001.

[5] B. E. Layton and A. M. Sastry. A mechanical model for collagen fibril load sharing in peripheral nerve of diabetic and nondiabetic rats. *Journal of Biomechanical Engineering*, 126(6):803–814, 2005.

[6] S. Pradhan, A. Hansen, and B. K. Chakrabarti. Failure processes in elastic fiber bundles. *Rev. Mod. Phys.*, 82:499–555, Mar 2010.

[7] J. Als-Nielsen and R. J. Birgeneau. Mean field theory, the ginzburg criterion, and marginal dimensionality of phase transitions. *American Journal of Physics*, 45(6):554–560, 1977.

[8] A. Hansen. Private communication.

[9] K. G. Wilson and M. E. Fisher. Critical exponents in 3.99 dimensions. *Phys. Rev. Lett.*, 28:240–243, Jan 1972.

[10] F. T. Pierce. Tensile tests for cotton yarns. *Journal of Textile Industry*, 17:355, 1926.

[11] P. C. Hemmer and A. Hansen. The distribution of simultaneous fiber failures in fiber bundles. *Journal of applied mechanics*, 59(4):909–914, 1992.

[12] H. E. Daniels. The statistical theory of the strength of bundles of threads. i. *Proceedings of the Royal Society of London A: Mathematical, Physical and Engineering Sciences*, 183(995):405–435, 1945.

[13] A. Hansen, P. C. Hemmer, and S. Pradhan. *The fiber bundle: modeling failure in materials*. Wiley, first edition, 2015.

[14] D. G. Harlow and S. L. Phoenix. The chain-of-bundles probability model for the strength of fibrous materials i: analysis and conjectures. *Journal of composite materials*, 12(2):195–214, 1978.

[15] G. G. Batrouni, A. Hansen, and J. Schmittbuhl. Heterogeneous interfacial failure between two elastic blocks. *Phys. Rev. E*, 65:036126, Feb 2002.

[16] R. C. Hidalgo, Y. Moreno, F. Kun, and H. J. Herrmann. Fracture model with variable range of interaction. *Phys. Rev. E*, 65:046148, Apr 2002.

[17] M. Kloster, A. Hansen, and P. C. Hemmer. Burst avalanches in solvable models of fibrous materials. *Phys. Rev. E*, 56:2615–2625, Sep 1997.

[18] S. D. Zhang and E. J. Ding. Burst-size distribution in fiber-bundles with local load-sharing. *Physics Letters A*, 193(5–6):425–430, 1994.

[19] A. Hansen and P. C. Hemmer. Burst avalanches in bundles of fibers: Local versus global load-sharing. *Physics Letters A*, 184(6):394–396, 1994.

[20] J. Hoshen and R. Kopelman. Percolation and cluster distribution. i. cluster multiple labeling technique and critical concentration algorithm. *Phys. Rev. B*, 14:3438–3445, Oct 1976.

[21] T. H. Cormen, C. E. Leiserson, R. L. Rivest, and C. Stein. *Introduction to Algorithms.* MIT Press, third edition, 2009.

[22] S. Sinha. Private communication.

[23] D. Stauffer and A. Aharony. *Introduction To Percolation Theory.* CRC press, 1994.

A Article

This appendix contains an article that has been submitted to Physical Review Letters (PRL), the way it looks as of May 15, 2015. It uses some of the results from this thesis: the averaged LLS strain curves in three, four and five dimensions for $P(x) = x$ and $P(x) = 1 - \exp(-x)$.

The local load sharing fiber bundle model in higher dimensions

Santanu Sinha,[1, 2, *] Jonas T. Kjellstadli,[2, †] and Alex Hansen[2, ‡]
[1] *Department of Physics, University of Oslo, P. O. Box 1048 Blindern, N-0316 Oslo, Norway*
[2] *Department of Physics, Norwegian University of Science and Technology, N-7491 Trondheim, Norway*
(Dated: April 29, 2015)

We consider the local load sharing fiber bundle model in one to five dimensions. Depending on the breaking threshold distribution of the fibers, there is a transition where the fracture process becomes localized. In the localized phase, the model behaves as the invasion percolation model. The difference between the local load sharing fiber bundle model and the equal load sharing fiber bundle model vanishes with increasing dimensionality with the characteristics of a power law.

PACS numbers: 46.50.+a 62.20.M- 81.40.Np

The fiber bundle model has come a long way since its introduction in 1926 by Peirce [1]. Initially introduced to model the strength of yarn, the model has slowly gained ground as a model for fracture in somewhat the same way that the Ising model has become a paradigm for magnetic systems. In 1945, Daniels' paper [2] on the fiber bundle model led to a continuous interest for the model in the mechanics community. The statistical physics community "discovered" the model in the early nineties in the aftermath of the surge of interest in fracture and in that community [3, 4].

The Peirce fiber bundle model is today known as the *equal load sharing* (ELS) fiber bundle model. N Hookean springs — fibers — of length x_0 and spring constant κ are placed between two parallel infinitely stiff clamps. When the distance between the clamps is $x_0 + x$, each fiber carries a load $\sigma = \kappa x$. Each fiber i has a maximum elongation threshold x_i, drawn from a probability density $p(x_i)$, upto which it can sustain before failing permanently. So the corresponding maximum load it can sustain is therefore $\sigma_i = \kappa x_i$. When a fiber fails, its load is shared equally among the surviving fibers since the clamps are infinitely stiff — hence "equal load sharing."

The *local load sharing* (LLS) fiber bundle model was introduced by Harlow and Phoenix [5, 6] as a one-dimensional array of fibers, each having an independent breaking threshold drawn from some threshold distribution $p(x)$. They defined the force redistribution rule as follows: When a fiber fails, the load it carried is redistributed in equal portions onto its two nearest surviving neighbors. Hence, if a fiber i is adjacent to $n_{l,i}$ failed fibers to the left and $n_{r,i}$ failed fibers to the right, it will carry a load [7]

$$\sigma_i = \kappa \left[1 + \frac{n_{l,i} + n_{r,i}}{2} \right] x \ , \tag{1}$$

where x is the distance between the clamps if all fibers were intact [4].

Where the ELS fiber bundle model is extreme in the sense that it redistributes the force carried by the failed fibers equally among all surviving fibers wherever they are placed, the LLS fiber bundle model is extreme in the opposite sense: only the nearest survivors, pick up the force carried by the failed fiber. There are many models that are intermediate between the two extreme models. For example, the γ model of Hidalgo et al. [8] distributes the force carried by the failed fiber according to a power law in the distance from the failed fiber. The soft clamp model [9–12] replaces one of the infinitely stiff clamps in the ELS model by a clamp with finite elastic constant. Hence, the load redistribution is governed by the elastic response of the soft clamp.

We emphasize the following subtle point in the implementation of the LLS model [4]. If the redistribution of forces after the failure of a fiber proceeds by dividing the force it carried in two and adding each half to the two nearest surviving fibers to the left and right — i.e., according to the recipe of Harlow and Phoenix [5] — the force distribution will not follow Eq. (1). Rather, it will become dependent on the order in which the fibers have failed. Hence, it will not be possible to determine the force distribution among the fibers only from the knowledge of present failed fibers in the system. This history dependency in the force distribution is unphysical. As an example, if two adjacent fibers have failed and the two nearest surviving fibers each has one survivor, the procedure will produce the following load distribution: $(7/4, 0, 0, 9/4)$ or $(9/4, 0, 0, 7/4)$ depending on the order in which the two middle fibers were failed. According to Eq. (1), the load distribution should be $(2, 0, 0, 2)$ independent of the order in which the fibers failed.

When implementing the LLS model in two or more dimensions, the force redistribution algorithm becomes even more crucial. We insist that the model should be physical where the force distribution among the surviving fibers can be determined by only knowing which fibers are already failed and it should not depend on the order in which they have failed. This leads to the concept of clusters of failed fibers, where the term "cluster" is used in the same sense as in the site percolation problem [13]: failed fibers that are nearest neighbors to each other form a cluster. The total load carried by all the failed fibers in a given cluster will then be shared equally by the surviving fibers that form the perimeter to that cluster. If

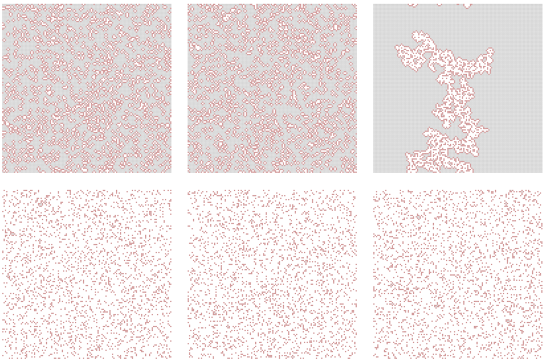

$p(x) = 1$ $p(x) = \exp(-x)$ $p(x) = \exp(-x + 1)$

FIG. 1. (Color online) Snapshots of the two-dimensional LLS model after 1792 failed fibers (top row) and after 13824 failed fibers (bottom row) with different threshold distributions for a 128 × 128 system. The red fibers are survivors adjacent to clusters of failed fibers, the gray fibers are survivors that are not adjacent to failed fibers and white fibers have failed.

a surviving fiber is adjacent to two different clusters of failed fibers, the total load it carries is the sum of the loads contributed from both the clusters.

This generalization of the one-dimensional LLS model to higher dimensions is the simplest one that ensures history independence in the force distribution. A more elaborate generalization may be found in Patinet et al. [14]. Here, one of the clamps is exchanged for a stretchable membrane that has no bending resistance. The elastic response of this model is equivalent to the LLS model in one dimension. However, it differs from the one we propose here in two dimensions.

We show in Fig. 1 the two stages of the two-dimensional LLS model: after 1792 (top row) and after 13824 (bottom row) failed fibers. $N = 128^2$ fibers, placed at the sites of a square lattice with periodic boundary conditions in all directions, are seen from above. The failed fibers are shown as white, the intact fibers that belong to the external and internal perimeters of the clusters of failed fibers are shown as red and other intact fibers are shown as gray. In the first column of the figure, the threshold distribution $p(x)$ was uniform on the unit interval. Hence, the cumulative probability was $P(x) = x$ where $x \in [0, 1]$. In the next two columns, the cumulative threshold probability was $P(x) = 1 - \exp(x_< - x)$ where $x \in [x_<, \infty)$ with $x_< = 0$ and $x_< = 1$ respectively. In the top row, it is hard to distinguish the difference between the first two panels of the figure. However, the third panel in the top row is very different. In this case, the breakdown process is *localized* from the very beginning. That is, a single cluster of failed fibers forms and keeps growing. On the other hand, three panels in the bottom row are all very similar.

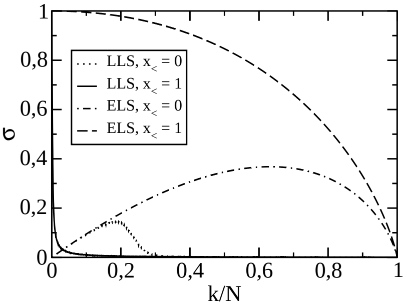

FIG. 2. Force per fiber σ as a function of the relative number of failed fibers k/N in the one-dimensional local load sharing model together with the ELS model result (Eq. 5). The thresholds were distributed according to $p(x) = \exp(-x + x_<)$ where $x \in [x_<, \infty)$ with $x_< = 0$ and 1 respectively. Here $N = 4000$. Each data series is based on 2000 samples.

When the breakdown process is localized so that only one cluster of failed fibers forms, the model is equivalent to the *invasion percolation model* [15]. In the invasion percolation model, each site is given a random number. An initial site is invaded. The perimeter of this one-site cluster form the growth sites and the growth site with the smallest random number associated with it is invaded. This is repeated, letting the perimeter of the cluster of invaded sites to be the growth sites. In the LLS model, the perimeter of the single cluster of failed fibers will carry the extra force that makes these and only these fibers liable for failure when the threshold is narrow enough to imply localization. It will be the fiber in the perimeter that has the smallest failure threshold that will fail next. Hence, it behaves precisely as the invasion percolation model.

We now consider the breaking characteristics of the LLS model in comparison to the ELS model. When k fibers have failed, the force F carried by the surviving fibers in the ELS model is

$$F = N\sigma = (N - k)\, \kappa\, x\ , \tag{2}$$

where we have defined the applied force per fiber $\sigma = F/N$. In the LLS model, we have

$$F = N\sigma = N\, \kappa\, x\ , \tag{3}$$

since the surviving perimeter fibers precisely absorb the load carried by the failed fibers.

We order the failure thresholds of the N fibers in an ascending sequence, $x_{(1)} < x_{(2)} < \cdots < x_{(k)} < \cdots < x_{(N)}$. According to order statistics [16], the average (over samples) of the kth member of this sequence is given by

$$P\left(\langle x_{(k)} \rangle\right) = \frac{k}{N} \tag{4}$$

for large N. We combine this equation with Eq. (2) for the ELS model assuming that $P(x) = 1 - \exp(-x + x_<)$

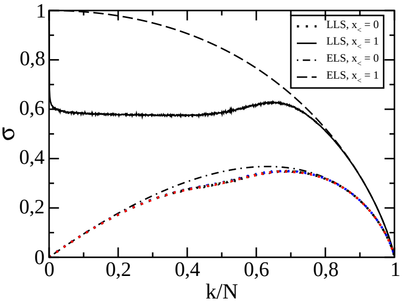

FIG. 3. (Color online) Force per fiber σ as a function of the relative number of failed fibers k/N in the two-dimensional LLS model compared with the ELS model result. The threshold distribution was $p(x) = \exp(x_< - x)$ where $x \in [x_<, \infty)$ with $x_< = 0$ and 1. LLS results for $x_< = 0$ (the lowermost curve) are also compared for different system sizes, $N = 32^2$ (blue), 64^2 (green), 128^2(red), and 256^2 (black), and they fall exactly on each other showing that the results are free from finite-size effects. For $x_< = 1$, $N = 256^2$. Each data series is based on 5000 samples.

for $x \in [x_<, \infty)$ to find

$$\sigma = \kappa \left[1 - \frac{k}{N}\right] \left[x_< - \ln\left(1 - \frac{k}{N}\right)\right] . \tag{5}$$

For a uniform threshold distribution in $[x_<, 1]$, the cumulative probability is $P(x) = (x - x_<)/(1 - x_<)$ we find

$$\sigma = \kappa \left[1 - \frac{k}{N}\right] \left[x_< + (1 - x_<)\frac{k}{N}\right] . \tag{6}$$

We show the ELS behavior for the exponential threshold distribution (Eq. 5) in Fig. 2 together with the corresponding curves ($x_< = 0$ and $x_< = 1$) for the LLS model in one dimension. There is a large difference between ELS and LLS models.

This picture changes in two dimensions. In Fig. 3, we show the results for the two-dimensional LLS model for exponential threshold distribution with cumulative threshold probabilities $P(x) = 1 - \exp(x_< - x)$ where $x \in [x_<, \infty)$ with $x_< = 0$ and 1. When comparing this figure to the corresponding one for one dimension (Fig. 2), we see that the LLS model now is much closer to the ELS model than in one dimension.

It should be pointed out that σ vs. k/N for the exponential threshold distribution with $x_< = 1$ has a curious upwards bend before its maximum value, see Fig. 3. We have also observed small upwards bend for the uniform threshold distribution with $x_< = 0.4$. This means that the model is stable in this region in the sense that if σ is used as the control parameter, fiber failures will only occur if σ is increased. This is not true in the ELS model. Hence, the LLS model is in fact *more stable* than the ELS model in this region.

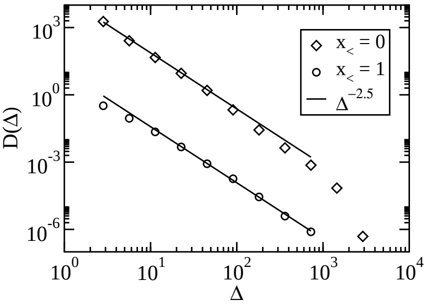

FIG. 4. The burst distribution in the two-dimensional LLS model. The threshold distribution was $p(x) = \exp(x_< - x)$ where $x \in [x_<, \infty)$. The data sets are based on 5000 samples of size $N = 256^2$.

The similarity between the ELS and LLS models is also evident in other quantities that characterize the two models. In Fig. 4 we show the burst distribution for the LLS model in two dimensions for the cumulative threshold probability $P(x) = 1 - \exp(x_< - x)$ where $x \in [x_<, \infty)$ with $x_< = 0$ and 1. The burst distribution is the histogram of the number of simultaneously failing fibers Δ when the force σ is the control parameter. Hemmer and Hansen showed in 1992 that the burst distribution in the ELS model is given by

$$\omega(\Delta) \sim \Delta^{-5/2} , \tag{7}$$

for a very wide class of threshold distributions to which $p(x) = \exp(x_< - x)$ belongs [17].

Later, Hansen and Hemmer investigated the burst distribution in the one-dimensional LLS model finding a burst exponent ≈ 4.5 rather than 5/2 [18]. Kloster *et. al.* [7] showed analytically that the burst distribution falls off faster than a power law in the LLS model when the threshold distribution is uniform on the unit interval. Fig. 4 shows that the burst distribution in the two-dimensional LLS model is consistent with Eq. (7) for $p(x) = \exp(x_< - x)$ where $x_< = 0$ or $x_< = 1$.

In Fig. 5, we show the σ vs. k/N curves for the *three-dimensional*, *four-dimensional* and *five-dimensional* LLS fiber bundle model for the cumulative threshold probability $P(x) = x$ with $x \in [0, 1]$ (top row) and $P(x) = 1 - \exp(x_< - x)$ with $x \in [x_<, \infty)$ (bottom row). We compare the curves with the ELS model results given in Eqs. (5) and (6). Interestingly, the curves for the LLS and the ELS models are approaching each other more and more as the dimensionality is increased. The difference in σ for LLS and ELS for different system dimensions is measured and plotted in Fig. 6 for the two threshold distributions.

It can be noticed that the maxima of the $\Delta\sigma$ curves shifts towards smaller k/N with changing dimensionality. Therefore, in order to quantify the difference between

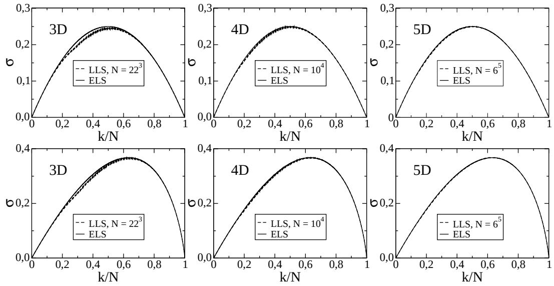

FIG. 5. Force per fiber σ as a function of the relative number of failed fibers k/N in the three-dimensional (3D), four-dimensional (4D) and five-dimensional (5D) LLS model. The top row corresponds to $P(x) = x$ with $x \in [0, 1]$ and bottom row corresponds to $P(x) = 1 - \exp(x_< - x)$ with $x \in [x_<, \infty)$. Each data series is averaged over atleast 40000 samples.

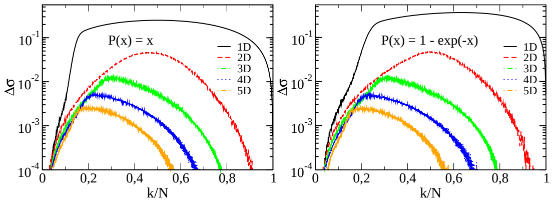

FIG. 6. (Color online) Difference between the force per fiber σ in the LLS and ELS models in one to five dimensions for the two threshold distributions. A rapid decrease in $\Delta\sigma$ can be observed with increasing dimensionality.

LLS and ELS models, we measure the total area ($\Delta\sigma_{\text{area}}$) under the $\Delta\sigma$ curves. In Fig. 7, we plot $\Delta\sigma_{\text{area}}$ as a function of the dimensionality D of the system. Interestingly, a power-law dependency

$$\Delta\sigma_{\text{area}} \sim D^{-\mu} \; , \tag{8}$$

with $\mu = 3.5 \pm 0.1$ is observed.

In the cases where the threshold cutoff is $x_< > 0$, there is a non-negligible N-dependency in the σ vs. k/N curves and the effective exponent μ needs further finite size scaling analysis to be determined.

From Eq. (8) we conclude that there is no finite upper critical dimension for which the LLS and ELS models become equal. However, the difference falls off rapidly with increasing D.

Finally, we like to highlight about the breaking process which makes the LLS and the ELS models similar at the earlier and at later stage of the breakdown when there is no localization. Early in the breakdown process, fibers fail not due to being under stress because they are on the perimeter of clusters of already failed fibers, but because they have small thresholds. Hence, we expect the LLS and the ELS models to be quite similar in all dimensions in this regime.

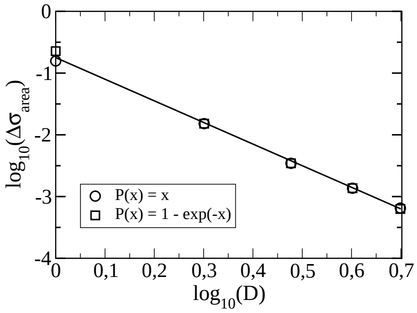

FIG. 7. The area under the $\Delta\sigma$ curves in Fig. 6 as a function of dimensionality D for the two different threshold distributions. The system sizes considered for 1 to 5 dimensions are 4000, 256^2, 22^3, 10^4 and 6^5 respectively.

As the breakdown process proceeds, the clusters of failed fibers merge and undergo a percolation transition. Essentially, all the remaining fibers become part of the perimeter of a single percolating cluster of failed fibers which can be seen in the bottom row of Fig. 1. Hence, as all the remaining fibers are adjacent to the same cluster, they share the same force as in the ELS fiber bundle model. Moreover, the threshold of percolation transition decreases with increasing dimensionality [13], which results in an increasing part of the ELS behavior. Therefore, as the dimensionality increases, the ELS and the LLS models must converge.

The LLS model is extreme in that it is the perimeter fibers that absorb the forces from the failed fibers. We have mentioned models that are in between the ELS and the LLS models. When the LLS and ELS models are rapidly approaching each other with increasing D, so will the in-between models also; they will rapidly approach the ELS model with increasing D. This argument also apply to models that normally are not classified as fiber bundle models, such as the fuse model where Zapperi *et. al.* [19] has reported a burst distribution exponent in three dimensions equal to 2.55, close to the ELS value 5/2. Hence, already in three dimensions, the ELS model is not far from the much more complex models of fracture.

We thank Per Christian Hemmer and Srutarshi Pradhan for numerous discussions on this subject. S.S. thanks the Norwegian Research Council for support through grant 216699.

---

[*] Santanu.Sinha@ntnu.no

[†] jonastk@stud.ntnu.no

[‡] Alex.Hansen@ntnu.no

[1] F. T. Peirce, J. Text. Ind. **17**, 355 (1926).
[2] H. E. Daniels, Proc. Roy. Soc. London **A183**, 405 (1945).
[3] S. Pradhan, A. Hansen and B. K. Chakrabarti, Rev.

Mod. Phys. **82**, 499 (2010).

[4] A. Hansen, P. C. Hemmer and S. Pradhan, *The fiber bundle: modeling failure in materials* (J. Wiley, Chichester, 2015).

[5] D. G. Harlow and S. L. Phoenix, J. Composite Mater. **12**, 195 (1978).

[6] D. G. Harlow and S. L. Phoenix, J. Mech. Phys. Solids **39**, 173 (1991).

[7] M. Kloster, A. Hansen and P. C. Hemmer, Phys. Rev. E **56**, 2615 (1997).

[8] R. C. Hidalgo, Y. Moreno, F. Kun and H. J. Herrmann, Phys. Rev. E **65**, 046148 (2002).

[9] G. G. Batrouni, A. Hansen and J. Schmittbuhl, Phys. Rev. E **65**, 036126 (2002).

[10] A. Stormo, K. S. Gjerden and A. Hansen, Phys. Rev. E **86**, R025101 (2012).

[11] K. S. Gjerden, A. Stormo and A. Hansen, Phys. Rev. Lett. **111**, 135502 (2013).

[12] K. S. Gjerden, A. Stormo and A. Hansen, Front. Phys. **2**, 66 (2014).

[13] D. Stauffer and A. Aharony, *Introduction to percolation theory* (Taylor and Francis, London, 1994).

[14] S. Patinet, D. Vandembroucq, A. Hansen and S. Roux, Europ. J. Phys. Spec. Top. **223**, 2339 (2014).

[15] D. Wilkinson and J. F. Willemsen, J. Phys. A **16**, 3365 (1983).

[16] E. J. Gumbel, *Statistics of extremes* (Dover Publ., Mineola New York, 2004).

[17] P. C. Hemmer and A. Hansen, ASME J. Appl. Mech. **59**, 909 (1992).

[18] A. Hansen and P. C. Hemmer, Phys. Lett. A **184**, 394 (1994).

[19] S. Zapperi, P. K. V. V. Nukala and S. Šimunović, Physica A **357**, 129 (2005).